JAERI-Research
2002-032

NUCLEAR DATA EVALUATION FOR ^{237}Np, ^{241}Am, ^{242g}Am AND ^{242m}Am IRRADIATED BY NEUTRONS AND PROTONS AT ENERGIES UP TO 250 MeV

December 2002

A.Yu. KONOBEYEV, Tokio FUKAHORI
and Osamu IWAMOTO

日本原子力研究所
Japan Atomic Energy Research Institute

本レポートは、日本原子力研究所が不定期に公刊している研究報告書です。
入手の問合わせは、日本原子力研究所研究情報部研究情報課（〒319-1195　茨城県那珂郡東海村）あて、お申し越し下さい。なお、このほかに財団法人原子力弘済会資料センター（〒319-1195　茨城県那珂郡東海村日本原子力研究所内）で複写による実費頒布を行っております。

This report is issued irregularly.
Inquiries about availability of the reports should be addressed to Research Information Division, Department of Intellectual Resources, Japan Atomic Energy Research Institute, Tokai-mura, Naka-gun, Ibaraki-ken 〒319-1195, Japan.

編集兼発行　日本原子力研究所

JAERI－Research 2002－032

Nuclear Data Evaluation for ^{237}Np, ^{241}Am, ^{242g}Am and ^{242m}Am Irradiated by Neutrons and Protons at Energies up to 250 MeV

A.Yu. KONOBEYEV, Tokio FUKAHORI and Osamu IWAMOTO

Department of Nuclear Energy System
Tokai Research Establishment
Japan Atomic Energy Research Institute
Tokai-mura, Naka-gun, Ibaraki-ken

(Received October 18, 2002)

Evaluation of nuclear data has been performed for ^{237}Np, ^{241}Am, ^{242g}Am and ^{242m}Am. Neutron data were obtained at energies from 20 to 250 MeV and combined with JENDL-3.3 data at 20 MeV. Evaluation of the proton data has been done from 1 to 250 MeV. The coupled channel optical model was used to obtain angular distributions for elastic and inelastic scattering and transmission coefficients. Pre-equilibrium exciton model and Hauser-Feshbach statistical model were used to describe neutron and charged particles emission from excited nuclei. These evaluation is the first work for producing full sets of evaluated file up to 250 MeV for ^{237}Np and Americium isotopes.

Keywords: Nuclear Data, Evaluation, Intermediate Energy, Neutron, Proton, Cross Section, Fission, Pre-equilibrium Model, Statistical Model, ^{237}Np, ^{241}Am, ^{242g}Am, ^{242m}Am

^{237}Np, ^{241}Am, ^{242g}Am, ^{242m}Am に対する 250 MeV までの中性子及び陽子入射核データの評価

日本原子力研究所東海研究所エネルギーシステム研究部
A.Yu. KONOBEYEV・深堀　智生・岩本　修

(2002年10月18日受理)

^{237}Np, ^{241}Am, ^{242g}Am, ^{242m}Am に対する核データの評価を行った。中性子データは20から250 MeVのエネルギー領域で評価し、20 MeV で JENDL-3.3 とつなげた。陽子データの評価は 1 から 250 MeV の範囲で行った。チャンネル結合光学モデルを用いて、弾性、非弾性散乱断面積の角度分布及び透過係数を求めた。前平衡過程の励起子モデルと Hauser-Feshbach の統計モデルを使用し、励起原子核からの中性子及び荷電粒子の放出を求めた。本評価は 250MeV までの ^{237}Np 及びアメリシウム同位体に対する評価済ファイル作成として、初めてのものである。

東海研究所：〒319-1195 茨城県那珂郡東海村白方白根 2-4

Contents

目次

This is a blank page.

1. Introduction

The nuclear data evaluation at intermediate energies has the principal meaning for increasing of accuracy of data used in different applications. Such applications include developments of concepts of the accelerator-driven waste transmutation system, radiation therapy, isotope production for medicine, material research using the accelerators and others. In data evaluation special attention should be given for incident particle energies below 250 MeV, where application of codes based on the intranuclear cascade evaporation model and the QMD-model is rather questionable due to the physical limitations or the deviation of the calculated and measured nuclear reaction characteristics.

The goal of this work was to obtain the nuclear data for ^{237}Np, ^{241}Am, ^{242g}Am and ^{242m}Am suitable to study neutron transport, heating, change of nuclide composition of the nuclear fuel and for other applications in the whole energy range from thermal energy up to 250 MeV. Both neutrons and protons were considered as incident particles in the present work. The evaluation has been done with theoretical models, as semi-empirical and empirical approaches, whose validity has been approved based on the large number of experimental data. Neutron data at the energy 20 MeV were combined with new JENDL-3.3 evaluation. Proton data are obtained from 1 to 250 MeV.

2. Brief Description of the Nuclear Models and Codes used in the Present Work

Coupled-channel optical model has been used to provide total cross section, angular distributions for elastic and inelastic scattering, and to calculate transmission coefficients for neutrons and charged particles. Parameters of the optical potential were obtained to perform the calculations up to 250 MeV. The numerical calculations were carried out with ECIS96 code [1]. The Hauser-Feshbach statistical and pre-compound models realized in GNASH code [2] were used for the calculation of particle emission spectra and nuclide production cross sections.

Nuclear level density was obtained on the basis of generalized superfluid model with the parameters fitted to the cumulative number of low-lying levels and observed neutron resonance densities [3]. The expression for nuclear level density is written as follows

$$\rho(U,J,\pi) = \rho_{qp}(U',J,\pi)\,K_{vib}(U')\,K_{rot}(U'), \qquad (1)$$

where $\rho_{qp}(U',J,\pi)$ is the density of quasi-particle nuclear excitation [4], $K_{vib}(U')$ and $K_{rot}(U')$ are vibrational and rotational enhancement factors at the effective energy of excitation U'. The vibrational enhancement coefficient $K_{vib}(U')$ was calculated according to Ref.[3].

For the inner saddle and axially symmetric saddle deformation rotational enhancement factors were obtained as follows $K_{rot}(U') = \sigma_{\perp}^2$, for the asymmetric saddle point $K_{rot}(U') = 2\sqrt{2\pi}\,\sigma_{\perp}^2\,\sigma_{II}$, and for the outer saddle $K_{rot}(U') = 2\sigma_{\perp}^2$ [5], where $\sigma_{\perp}$ and σ_{II} are perpendicular and parallel spin cutoff functions. The attenuation of the rotational enhancement with the excitation energy growth was considered according to Refs.[3,6].

The nuclear level density parameters were calculated according to the following expression [3,4]

$$a(U) = \begin{cases} \tilde{a}\left(1+\delta W\,\varphi(U'-E_{cond})/(U'-E_{cond}\right), \text{if } U'> U_{cr} \\ a(U_{cr}), \qquad \text{if } U'< U_{cr} \end{cases}, \tag{2}$$

where the asymptotic value of level density parameter is equal to $\tilde{a} = A(\alpha+\beta A^{-1/3})$, α=0.073, β = 0.115, $\varphi(U) = 1-\exp(-\gamma U)$, $\gamma = 0.4/A^{1/3}$ MeV^{-1}, δW is the shell correction. The effective energy of excitation U', critical energy of the phase transition U_{cr} and the condensation energy E_{cond} were defined according to Refs.[3,4]. For the ground state the shell corrections δW_{gs} in Eq.(2) were calculated on the basis of Myers, Swiatecky approach [7]. For the inner and outer saddle points the values of δW_s^A and δW_s^B were taken from Ref.[5] considering the difference between types of the saddle symmetry.

The fission barriers were considered as spin-dependent and described as follows [8],

$$B_f^i(J) = C^i\,B_{ld}(J) + f(T)\,g(J)\,(\delta W_s^i - \delta W_{gs}), \tag{3}$$

where $B_{ld}(J)$ is the spin-dependent barrier calculated according to Sierk liquid-droplet model [9], δW_{gs} and δW_s^i are the shell corrections for ground state and the i-th saddle point, respectively, C^i is the adjustment factor, f(T) and g(J) are temperature and spin fade-out functions. Factors C^i were defined in the present work to provide an agreement between calculations and available experimental data for neutron interactions with uranium isotopes. The nuclear temperature fade-out function f(T) in Eq.(3) was calculated according to Ref.[8]:

$$f(T) = \begin{cases} 1, & \text{for } T \le 1.65\,\text{MeV} \\ 5.809\exp(-1.066\,T), & \text{for } T > 1.65\,\text{MeV} \end{cases}, \tag{4}$$

The function g(J) was defined according to the following expression [8]:

$$g(J) = \frac{1}{1+\exp(J-J_{1/2})/\Delta J}, \tag{5}$$

where the parameters $J_{1/2}$ and ΔJ are equal to $J_{1/2}$=24, ΔJ=2.5 [10]. Nuclear dissipation effects resulting in reduction of fission width with growth of excitation energy were taken into consideration based on the results of Refs.[11,12].

The pre-equilibrium nucleon spectra were calculated with exciton model. Values of averaged squared matrix element for two body interactions were obtained from Ref.[13], where the parameterization

of $<|M|^2>$ has been done as a function of E/n (where E is the excitation energy and "n" is the number of excitons). The description of the pre-compound model including angular momentum effects can be found in Refs.[2,14].

Multiple pre-compound emission has been considered. Certain improvement in the description of such emission has been done in the present work comparing with the GNASH algorithm [2]. The general expression for the second pre-equilibrium particle emission spectra calculation used in GNASH code has the following form [15]

$$\frac{d\sigma_j^{mpe}}{dE}=\sum_n\sum_{i=\pi,\upsilon}\int_{U=E+Q}^{U_{max}}\frac{d\sigma_i^{(n)}}{dU}\left(\frac{\omega(lp,0,E+Q)\,\omega(p-1,h,U-E-Q)}{p\;\omega(p,h,U)}R_{i,j}^{(n)}\right)T_j(E)\,dU \qquad (6)$$

where "i" and "j" is the type of the first and second pre-compound particle emitted, respectively; E is emission energy and Q is separation energy for "j"-particle; $d\sigma^{(n)}_i/dU$ is differential cross section of p-h state after pre-equilibrium emission of "i"-particle; $R^{(n)}_{i,j}$ is the neutron-proton distinguishability factor calculated according to Ref.[16]; $T_j(E)$ is the probability of the "j"-particle to escape with energy E; summing is for all "n"-exciton states and primary particle types.

Calculation of $T_j(E)$ from Eq.(6) in the GNASH code [2] is based on simple approximation considering s-wave transmission coefficient. The actual values used in the code are shown in Fig.1. In the present work the probability of particle emission, $T_j(E)$, is calculated as follows

$$T_j(E)=\frac{\lambda_j^e(E)}{\lambda_j^e(E)+\lambda_j^+(E+Q)}, \qquad (7)$$

where λ^e_j is the particle emission rate and λ^+_j is the intranuclear transition rate corresponding to the absorption of "j"-particle in nucleus. The emission and intranuclear transition rates are calculated according to the following relations

$$\lambda_j^e=\frac{(2S_j+1)\mu_j E\sigma_j^{inv}(E)}{\pi^2\hbar^3 g_j}, \qquad (8)$$

$$\lambda_j^+=V_j\,\sigma_j^{nn}(E+Q)\rho, \qquad (9)$$

where S_j and μ_j are the spin and the reduced mass of "j"-particle, σ^{inv}_j, is the inverse reaction cross section, g_j is the single level density, V_j is the velocity of the particle of "j"-type inside the nucleus, σ^{nn}_j is the nucleon-nucleon interaction cross section corrected for the Pauli principle, ρ is the nuclear density. Calculation of $T_j(E)$ according to Eqs.(7)-(9) corresponds to the basic assumptions of the hybrid exciton model [16,17]. Values of $T_j(E)$ calculated in such a way are shown in Fig.1 for neutrons and protons. An example of particle spectra calculated with the $T_j(E)$ values obtained by Eqs.(7)-(9) is shown in Fig.2 for ^{209}Bi(p,p') reaction at the incident proton energy equal to 62 MeV. The experimental data are taken from Ref.[18]. The use of Eqs.(7)-(9) improves an agreement with experimental data as shown in Fig.2.

The model used in the original GNASH code [2] to describe the pre-compound spectra of the composite particles contains the noticeable shortcomings. The example is given in Fig.3. This figure shows the α-particle spectra for p+^{209}Bi reaction at the primary energy E_p=90 MeV, calculated on the basis of the approach described in Ref.[2] and with pre-equilibrium model described below. The calculations with GNASH code are not in good agreement with the available experimental data [19]. It should be noted that any variation of the main parameters of pre-equilibrium model [2] could not provide a reasonable agreement with experimental data for complex particle emission from heavy nuclei. The shortcomings of the GNASH algorithm [2] for description of the pre-compound emission for the particles with $A \geq 2$ were pointed out also in Ref.[20].

In the present work pre-equilibrium α-particle emission spectra were calculated in the framework of coalescence pick-up model [21] combined with the knock-out model as shown in Refs.[22,23]. Multiple pre-equilibrium emission was taken into consideration. For deuteron, triton and ^{3}He spectra calculation the exciton pick-up model [24] was applied. Contribution of direct mechanism to deuteron emission was considered on the basis of phenomenological approach [25]. All approaches considered above were tested using available experimental data in the intermediate energy region of primary particles.

Fission neutron and γ-spectra were obtained on the basis of the model described in Ref.[26]. This model is the refined Fong approach [27] adjusted to experimental data for fission fragment yields and other fission characteristics in the wide energy range of primary particles. The algorithm described in Ref.[26] was used before as the part of the intranuclear cascade evaporation code [28]. In the present work to increase accuracy of the obtained results this algorithm was introduced in ALICE code [29,30], which is at the same time the modified and extended version of the original Blann code [31]. Application of this code (ALICE/ASH) allows to use more sophisticated models, such as optical model for inverse cross sections and superfluid model for nuclear level density calculations, comparing with the approaches usually used in the codes based on the INC model.

3. ^{237}Np

3.1 Neutron Data Evaluation

Total, elastic and reaction cross sections calculated in the present work with coupled-channel model are shown in Figs.4-6 in comparison with systematics predictions [32, 33] and JENDL-3.3 data. Neutron elastic and inelastic scattering angular distributions for the selected excited levels are shown in Figs.7-9 at the primary neutron energy equal to 20 MeV together with the data from JENDL-3.3, ENDF/B-VI and CENDL-2. The calculated elastic scattering distribution for E_n=50, 100 and 250 MeV is presented in Fig.10. Figure 11 shows the direct neutron inelastic scattering cross sections calculated for the excited levels $7/2^+$ and $9/2^+$ at the energies up to 250 MeV.

Fission cross sections calculated with GNASH and ALICE/ASH codes are compared in Fig.12 with Fukahori's systematics predictions [33], evaluated data in Ref.[34] and experimental data [35-39]. The evaluated (n,f) reaction cross section is shown in Fig.13 at the energies up to 250 MeV. Figure 14 shows the evaluated (n,f) cross section in more detail at the energies up to 50 MeV. Contributions of nuclides with different Z in (n,f) cross section is presented in Fig.15.

Neutron production cross section calculated by GNASH and ALICE/ASH codes without the consideration of the post-fission evaporation is shown in Figs.16 and 17. Contributions of different nuclei in neutron production is shown in Fig.18 Figure 19 illustrates the neutron double-differential cross sections calculated by GNASH code at the primary neutron energies equal to 50–200 MeV. Evaluated (n,xn) reaction cross sections are shown in Fig.20. Figures 21 and 22 show the post-fission neutron characteristics. Comparison of total neutron production cross section for uranium isotopes and ^{237}Np is presented in Fig.23. Evaluated charged particle production cross sections are shown in Figs.24-30.

3.2 Proton Data Evaluation

Basic characteristics of the proton interaction with ^{237}Np evaluated in the present work are shown in Figs.31-40. Figure 31 shows the proton reaction cross section calculated using different sets of coupled-channel model parameters and evaluated according to the systematics from Ref.[32]. Calculated elastic scattering angular distribution is shown in Fig.32 for the primary proton energy equal to 10, 50 and 250 MeV.

Figure 33 shows the fission cross section calculated with GNASH and ALICE/ASH codes, the data measured in Refs.[40-44], the cross section estimated according to the systematics [33] and evaluated data in Ref.[34]. Data from Ref.[40] is cited in Ref.[45]. There is a good agreement between calculated and evaluated cross sections based on Refs.[33,34]. The ratio data of proton induced fission cross section (p,f) to neutron fission cross section (n,f) evaluated in the present work and are obtained in Ref.[46] are shown in Fig.34. Figures 35 and 36 illustrate contribution of different nuclei in total fission cross section (p,f) for ^{237}Np.

Neutron and proton production cross sections are shown in Figs.37-39. Charge particle production cross sections are shown in Fig.40.

4. Americium Isotopes with A=241 and 242

Basic features noted above for the neutron and proton interactions with Neptunium isotopes at the intermediate energies remain valid for Americium-241 and –242. The shape of the evaluated cross sections, particle spectra, Z- and A- dependence of integrated values, like as particle production cross section, are similar for various actinides considered in the present work. The examples are shown in Figs.41-48.

Figures 41 and 42 show neutron total and elastic scattering cross sections for ^{241}Am calculated by coupled-channel optical model, cross sections evaluated according to the systematics from Refs.[47,48] and data taken from JENDL-3.3. Fission cross section for ^{241}Am calculated with GNASH and ALICE/ASH codes is shown in Figs.43 and 44 together with measured data from Refs.[49,50], cross sections evaluated with Fukahori's systematics [33], JENDL-3.3 and ENDF/B-VI data. There is a good agreement among JENDL-3.3 data, cross section calculated by GNASH code and experimental data from Ref.[50]. The calculated result by GNASH code was adopted as a final evaluation. Neutron production cross section for ^{241}Am and ^{242g}Am are presented in Fig.45 for neutron induced reactions. Neutron induced fission cross section for ^{242g}Am and ^{242m}Am are compared in Fig.46. The main difference of cross sections is observed below 20 MeV. Recommended proton induced fission cross section and γ-production cross section for ^{241}Am and ^{242g}Am are shown in Figs.47 and 48. The corresponding cross sections for ^{242g}Am and ^{242m}Am are similar.

5. Conclusion

New data evaluation has been performed for ^{237}Np, ^{241}Am, ^{242g}Am and ^{242m}Am at the intermediate energies. For the first time the evaluation for actinides has been done for neutron and proton induced reactions at the energies up to 250 MeV.

The evaluation procedure has included applications of theoretical models and analyses of available experimental data. The coupled-channel optical model, pre-compound and equilibrium models were used for nuclear reaction characteristics calculation. Neutron data obtained were combined with the JENDL-3.3 data at the energy 20 MeV to get full data set at the energies from 10^{-5} eV to 250 MeV. The data for the proton induced reactions were evaluated in the energy region from 1 to 250 MeV.

Acknowledgements

Authors are grateful to Dr. S. Chiba, Research Group of Hadron Science, and members of Nuclear Data Center, for their valuable discussions. The author, A.Yu. Konobeyev, also thank Japan Atomic Energy Research Institute, for giving the opportunity to perform this work.

References

[1] J.Raynal, ECIS96 code, unpublished

[2] P.G.Young, E.D.Arthur, M.B.Chadwick, Comprehensive Nuclear Model Calculations: Theory and Use of the GNASH Code, Proc. Int. Atomic Energy Agency Workshop on Nuclear Reaction Data and Nuclear Reactors, April 15-May 17, 1996, v.1, p.227; Report LANL, LA-12343-MS (1992).

[3] A.V.Ignatyuk, Level Densities, In: Handbook for Calculations of Nuclear Reaction Data, IAEA-TECDOC-1034, p.65 (1998).

[4] A.V.Ignatyuk, K.K.Istekov, G.N.Smirenkin, *Yadernaja Fizika* **29**, 875 (1979).

[5] V.M.Maslov, Fission Level Densities, In: Handbook for Calculations of Nuclear Reaction Data, IAEA-TECDOC-1034, p.81 (1998).

[6] G.Hansen, A.Jensen, *Nucl. Phys.* **A406**, 236 (1983).

[7] W.O.Myers, W.J.Swiatecky, *Ark. Fysik* **36**, 343 (1967).

[8] A.D.Arrigo, G.Giardina, M.Herman, A.V.Ignatyuk, A.Taccone, *J. Phys. G: Nucl. Part. Phys.* **20**, 365 (1994).

[9] A.Sierk, *Phys. Rev.* **C 33**, 2039 (1986).

[10] M.Herman, EMPIRE-II Statistical Model Code for Nuclear Reaction Calculations (v.2.13 Trieste), April 5, 2000, unpublished.

[11] E.M.Rastopchin, S.I.Mulgin, Yu.V.Ostapenko, V.V.Pashkevich et al, *Sov. J. Nucl. Phys.* **53**, 741 (1991).

[12] A.V.Ignatyuk, G.A.Kudyaev, A.R.Junghans, M.deJong et al, *Nucl. Phys.* **A593**, 519 (1995).

[13] C.Kalbach, *Phys. Rev.* **C32**, 1157 (1985).

[14] M.B.Chadwick, P.G.Young, P.Oblozinsky, A.Marcinkowski, *Phys. Rev.* **C49**, R2885 (1994).

[15] M.B.Chadwick, P.G.Young. D.C.George, Y.Watanabe, *Phys. Rev.* **C50**, 996 (1994).

[16] M.Blann, H.Vonach, *Phys. Rev.* **C28**, 1475 (1983).

[17] M.Blann, *Phys. Rev. Lett.* **28**, 757 (1972).

[18] F.E.Bertrand, R.W.Peelle, *Phys. Rev.* **C8**, 1045 (1973).

[19] J.R.Wu, C.C.Chang, H.D.Holmgren, *Phys. Rev.* **C19**, 698 (1979).

[20] A.V.Ignatyuk, V.P.Lunev, Yu.N.Shubin, E.V.Gai, N.N.Titarenko, A.Ventura, W.Gudowski, *Nucl. Sci. Eng.* **136**, 340 (2000).

[21] A.Iwamoto, K.Harada, *Phys. Rev.* **C26**, 1821 (1982).

[22] A.Yu.Konobeyev, V.P.Lunev, Yu.N.Shubin, Pre-equlibrium Emission of Clusters, Report IPPE-2465 (1995).

[23] A.Yu.Konobeyev, V.P.Lunev, Yu.N.Shubin, *Acta Physica Slovaca* **45**, 705 (1995).

[24] N.Sato, A.Iwamoto, K.Harada, *Phys. Rev.* **C28**, 1527 (1983).

[25] A.Yu.Konobeyev, Yu.A.Korovin, *Kerntechnik* **61**, 45 (1996).

[26] A.Yu.Konobeyev, Yu.A.Korovin, M.Vecchi, *Kerntechnik* **64**, 216 (1999).

[27] P.Fong Statistical Theory of Nuclear Fission, (Gordon and Breach Science Publ., NY, 1969); P.Fong, *Phys. Rev.* **135B**, 1338 (1964).

[28] V.S.Barashenkov, A.Yu.Konobeyev, Yu.A.Korovin, V.N.Sosnin, *Atomnaja Energija* **87**, 283 (1999).

[29] A.Yu.Konobeyev, Yu.A.Korovin, P.E.Pereslavtsev, Code "ALICE/ASH" for Calculation of Excitation Functions, Energy and Angular Distributions of Emitted Particles in Nuclear Reactions, Report INPE, Obninsk, (1997).

[30] A.I.Dityuk, A.Yu.Konobeyev, V.P.Lunev, Yu.N.Shubin, New Advanced Version of Computer Code ALICE-IPPE, Report IAEA INDC(CCP)-410 (1998).

[31] Blann M. ALICE 87 (Livermore) Precompound Nuclear Model Code, Report IAEA-NDS-93 REV.O (1988).

[32] V.S.Barashenkov, A.Polanski, Electronic Guide for Nuclear Cross sections, JINR, Dubna, (1995).

[33] T.Fukahori, S.Pearlstein, Report BNL-45200 (1991).

[34] S.Yavshits, O.Grudzevich, G.Boykov, V.Ippolitov, Proc. of the 2000 Symposium on Nuclear Data, Nov. 16-17, 2000, Tokai, Japan, JAERI-Conf 2001-006, INDC(JPN)-188/U, p.277 (2001).

[35] V.M.Pankratov,N.A.Vlasov,B.V.Rybakov, *Atomnaya Energiya*, **9**, 399 (1960).

[36] V.M.Pankratov, *Atomnaya Energiya*, **14**, 177 (1963).

[37] J.W.Behrens, J.C.Browne, J.C.Walden, *Nucl. Sci. Eng.* **80**, 393 (1982).

[38] P.W.Lisowski, J.L.Ullmann, S.J.Balestrini, A.D.Carlson, O.A.Wasson, N.W.Hill, Proc. Int. Conf. for Nuclear Data for Science and Technology, Mito, May 30- June 3, 1988, p97.

[39] O.Shcherbakov, ISTC Project No.609, 2000.

[40] O.E.Shigaev, V.S.Bychenkov, M.F.Lomanov, A.I.Obukhov et al, Report Khlopin Radiev. Inst., Leningrad, Ri-17 (1973); M.F.Lomanov, G.G.Shimchuk, R.M.Yakovlev, *Health Phys.* **37**, 677 (1979).

[41] A.N.Smirnov, I.Yu.Gorshkov, A.V.Prokofiev, V.P.Eismont, Proc. 21st Intern. Symp. on Nuclear Phys., Gaussig, Germany, November 4-8, 1991, p.214; V.P.Eismont, A.V.Prokofiev, A.N.Smirnov, Proc. Int. Conf. for Nuclear Science and Technology, Gatlinburg, May 9-13, 1994, p.397.

[42] T.Ohtsuki, Y.Nagame, K.Tsukada, N.Shinohara et al, *Phys. Rev.* **C44**, 1405 (1991).

[43] V.A.Konshin, E.S.Matusevich, V.I.Regushevski, *Yadernaja Fizika* **4**, 97 (1966).

[44] P.Polak, A.H.W.Aten, *J. Inorg. Nucl. Chem.*, **42**, 641 (1980).

[45] V.P.Eismont, A.V.Prokofiev, A.N.Smirnov, Proc. Int. Conf. for Nuclear Science and Technology, Gatlinburg, May 9-13, 1994, p.397.

[46] V.P.Eismont, A.V.Prokofiev, I.V.Ryzhov, A.N.Smirnov et al, "Up-to-Date Status and Problems of the Experimental Nucleon-Induced Fission Cross section Data Base at Intermediate Energies,

Proc. Int. Conf. on Accelerator-Driven Transmutation Technologies and Applications (ADTTA), Prague, Czech Republic, June 7-11, 1999, text distributed on CD, P-C23.

[47] P.G.Young, Experience at Los Alamos with Use of the Optical Model for Applied Nuclear Data Calculations, In: Handbook for Calculations of Nuclear Reaction Data, IAEA-TECDOC-1034, p.131 (1998).

[48] V.S.Barashenkov Cross sections of Interactions of Particle and Nuclei with Nuclei, JINR, Dubna (1993); http://www.nea.fr/html/dbdata/bara.html

[49] J.W.Behrens, J.C.Browne, *Nucl. Sci. Eng.* 77, 444 (1981).

[50] J.W.T.Dabbs, C.H.Johnson, C.E.Bemis, *Nucl. Sci. Eng.* 83, 22 (1983).

[51] V.S.Bychenkov, M.F.Lomanov, A.I.Obukhov, G.G.Shimchuk, R.M.Yakovlev, 1989, 1992, cited by [34].

[52] A.Yu.Konobeyev, Yu.A.Korovin, *Atomic Energy* 85, 556 (1998) (translated from Russian Journal "*Atomnaja Energija*").

[53] R.F.Coleman, B.E.Hawker, L.P.O'connor, J.L.Perkin, *Proceedings of the Physical Society (London)* 73, 215 (1959).

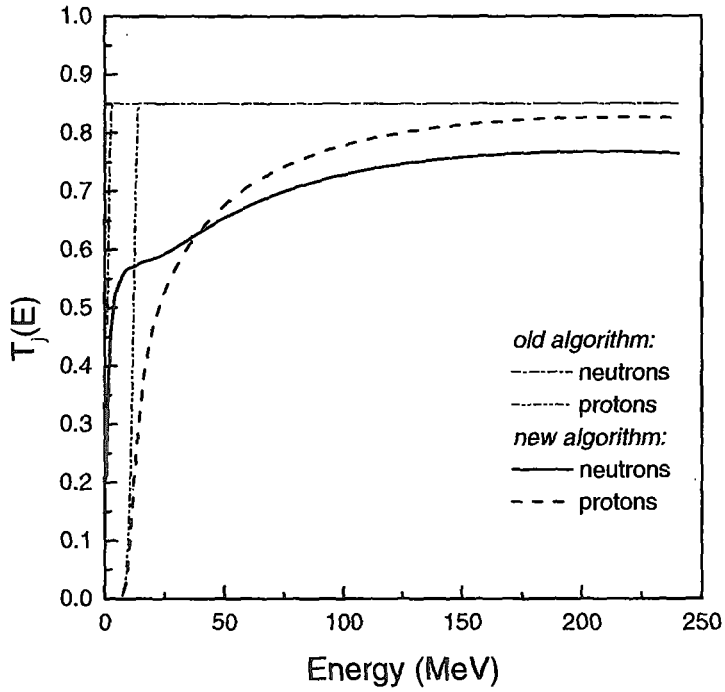

Fig.1 Emission probability of nucleons calculated as described in Ref.[2] ("old algorithm") and with Eqs.(6)-(9) ("new algorithm").

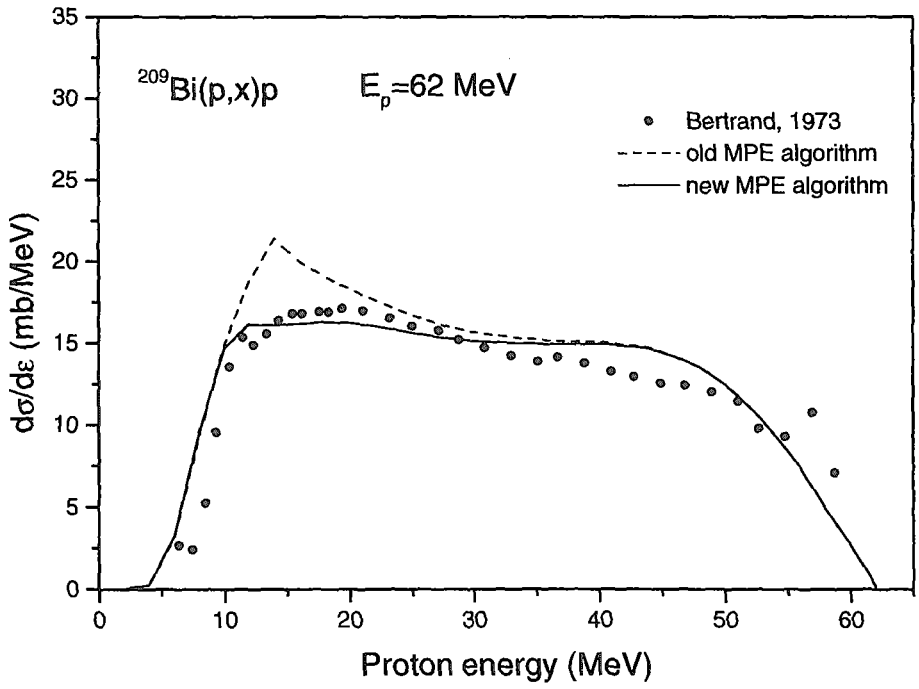

Fig.2 Energy distribution of secondary protons in p+^{209}Bi interactions at the energy E_p=62 MeV calculated using new algorithm (solid line) and old one (dashed line) for $T_j(E)$ calculation. The experimental data are from Ref.[18].

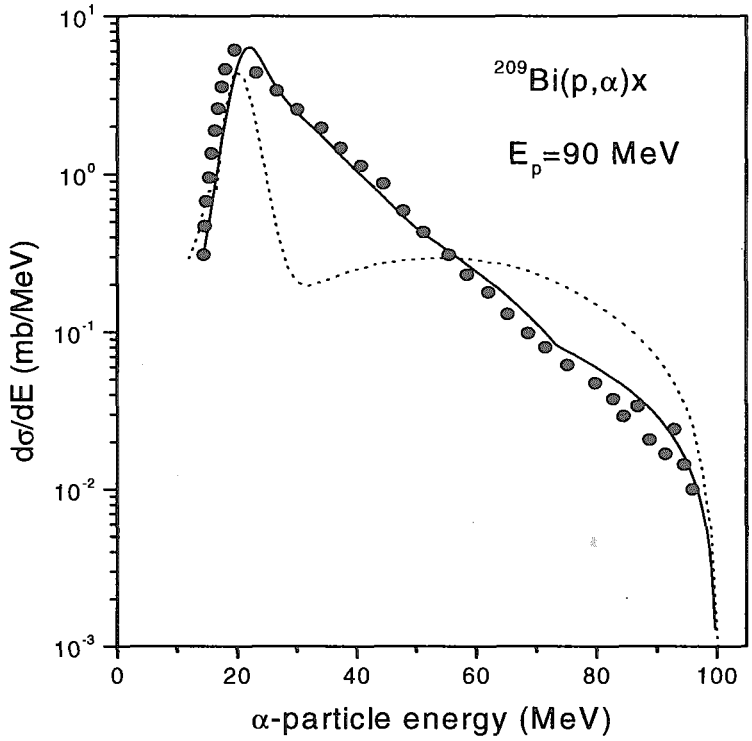

Fig.3 α-particle spectra for p+^{209}Bi reaction at E_p=90 MeV calculated using pre-compound model for complex particle emission [2] (dotted line) and with approach described in the present work (solid line). The experimental data are from Ref.[19].

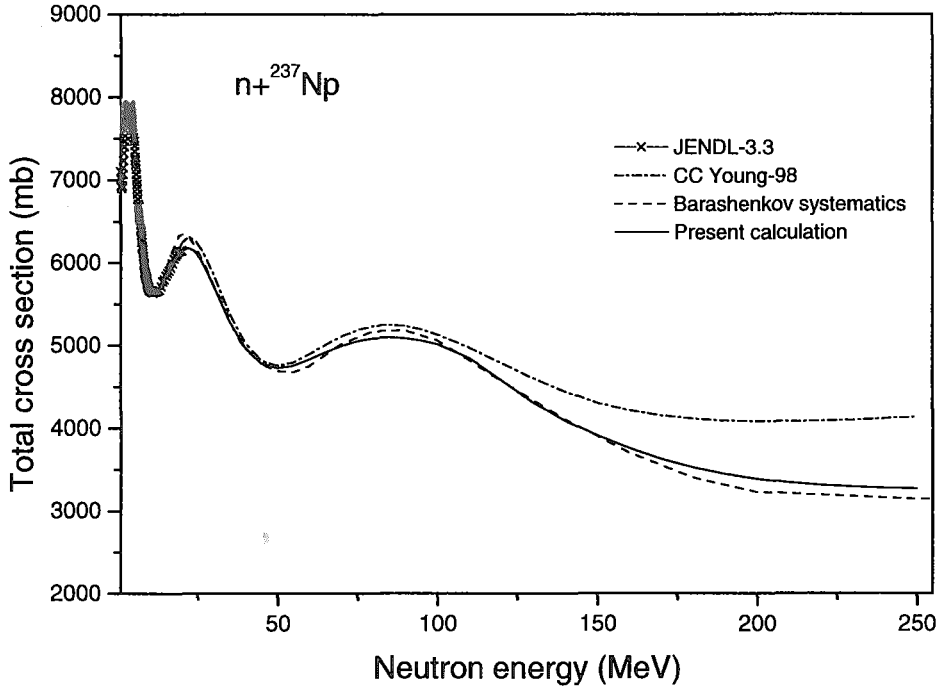

Fig.4 Total neutron cross section for ^{237}Np calculated using different sets of coupled-channel optical model parameters, evaluated according to Ref.[32] and taken from JENDL-3.3.

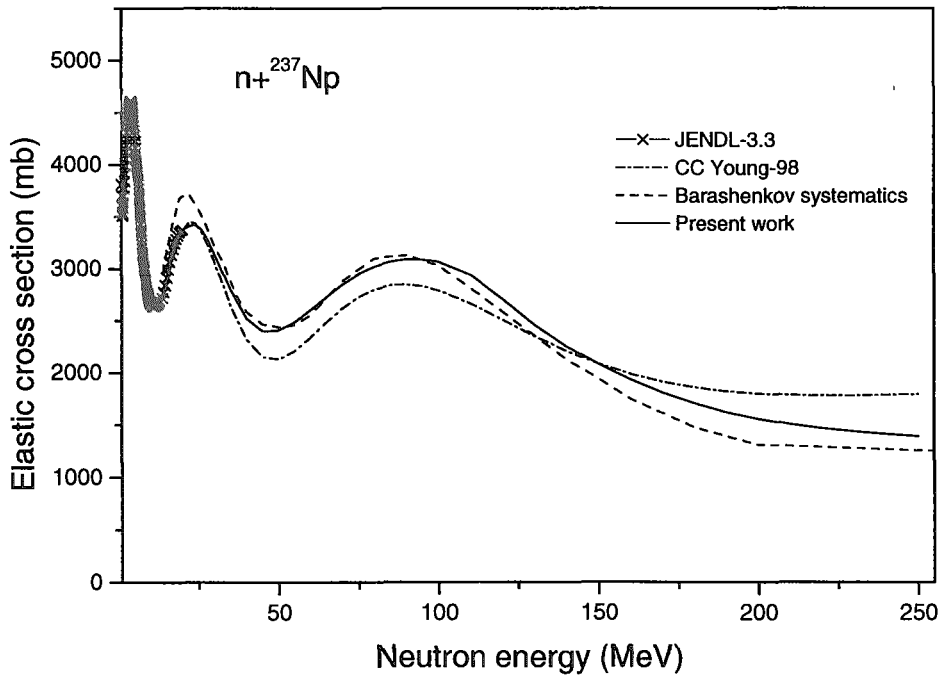

Fig.5 Neutron elastic scattering cross section for ^{237}Np calculated using different sets of the coupled channel optical model parameters, evaluated according to Ref.[32] and taken from JENDL-3.3.

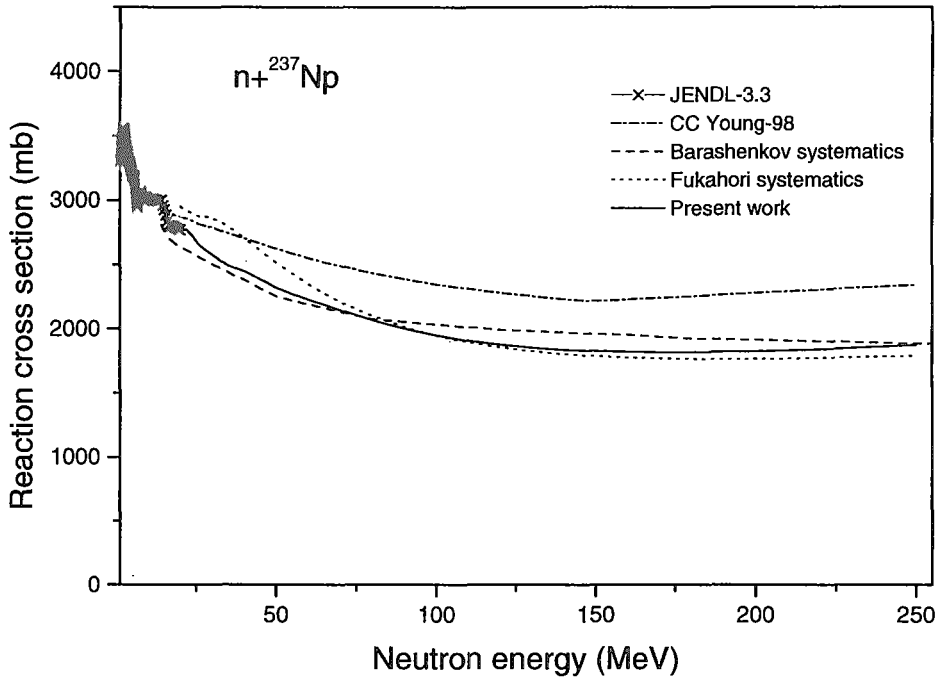

Fig.6 Neutron reaction cross section for ^{237}Np calculated using different sets of coupled-channel optical model parameters, evaluated according to Refs.[32,33] and taken from JENDL-3.3.

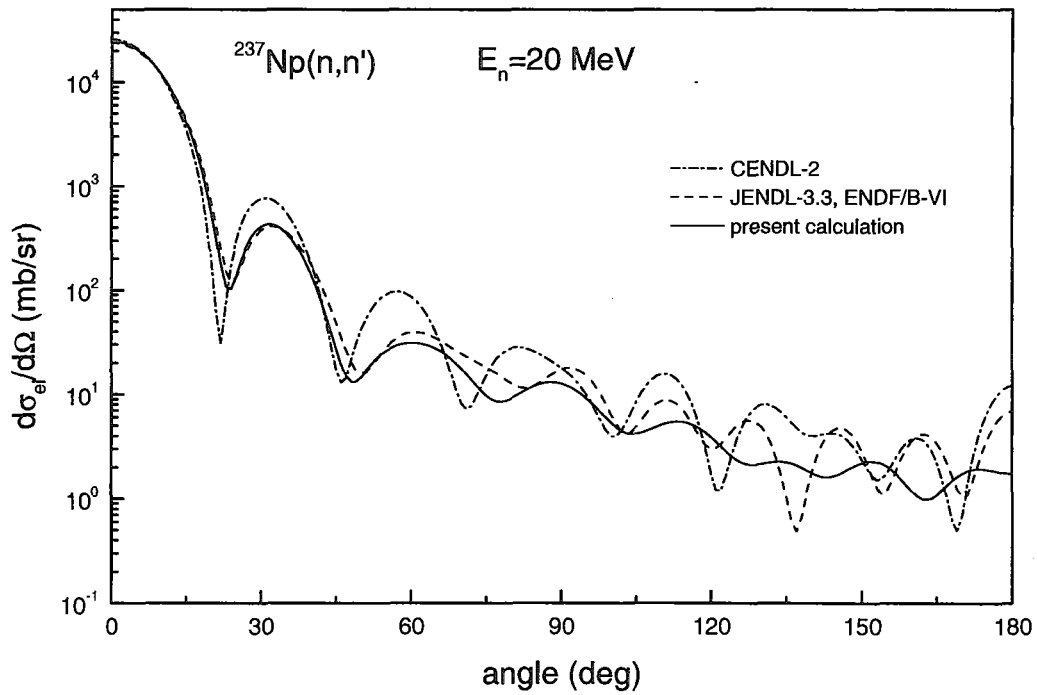

Fig.7 Elastic scattering angular distributions for ^{237}Np at the primary neutron energy E_n = 20 MeV obtained in the present work and taken from different evaluated nuclear data libraries.

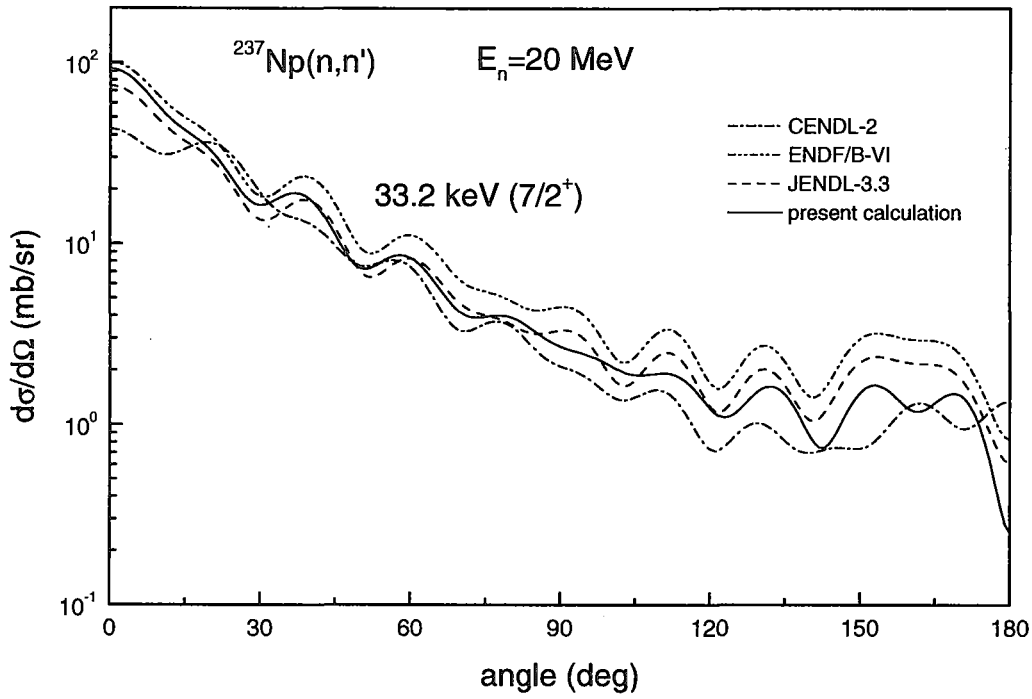

Fig.8 Neutron inelastic scattering angular distributions for ^{237}Np at the primary energy E_n = 20 MeV for the excited level 33.2 keV (7/2$^+$) obtained in the present work and taken from different data libraries.

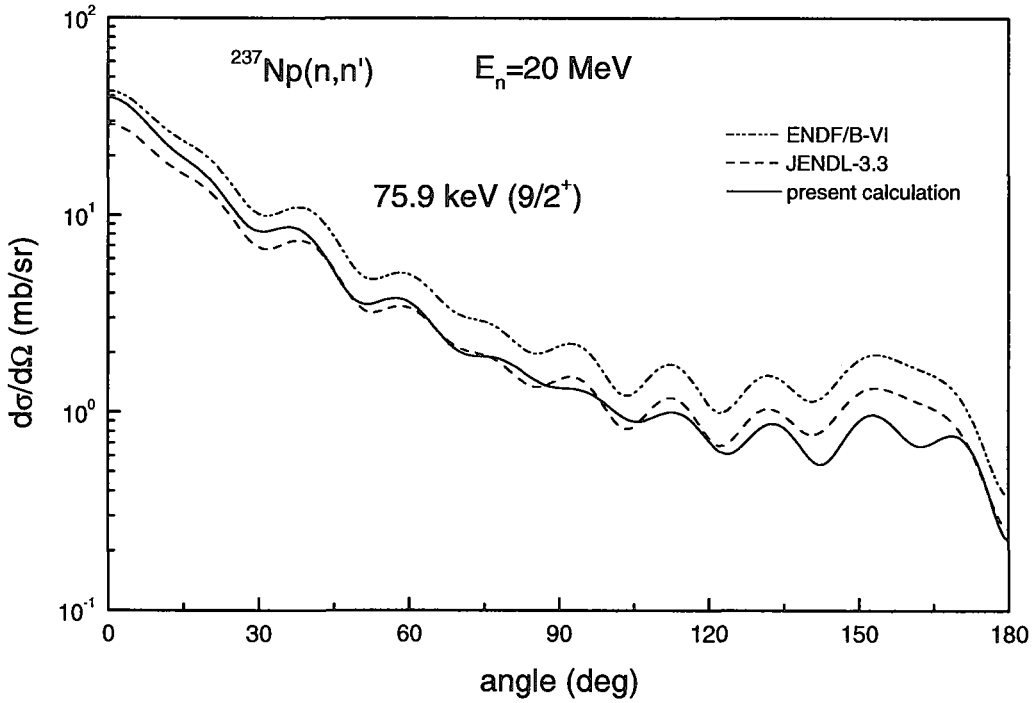

Fig.9 Neutron inelastic scattering angular distributions for ^{237}Np at the primary energy E_n = 20 MeV for the excited level 75.9 keV (9/2$^+$) obtained in the present work and taken from different data libraries.

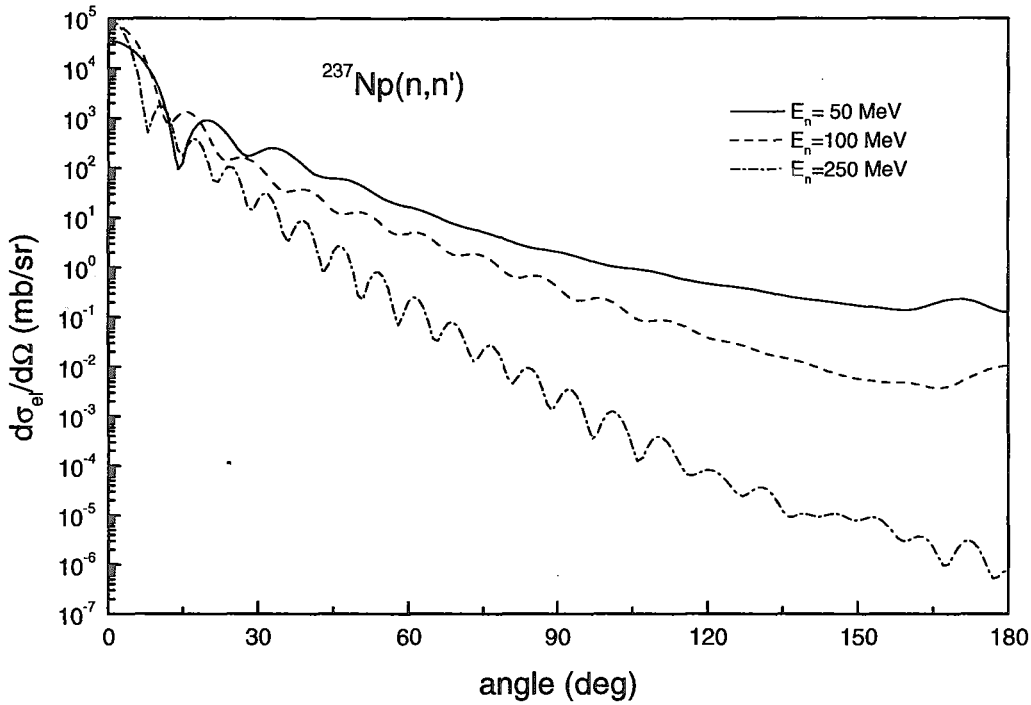

Fig.10 Elastic scattering angular distributions for ^{237}Np at different neutron incident energies calculated in the present work.

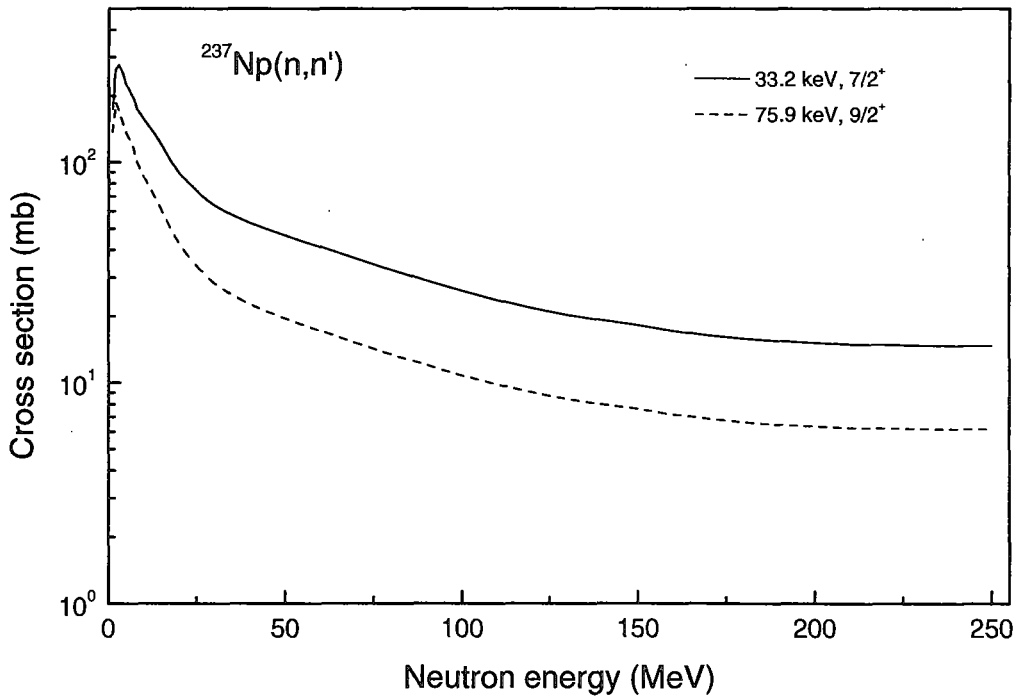

Fig.11 Direct neutron inelastic scattering cross sections calculated for ^{237}Np for the excited levels 7/2$^+$ and 9/2$^+$.

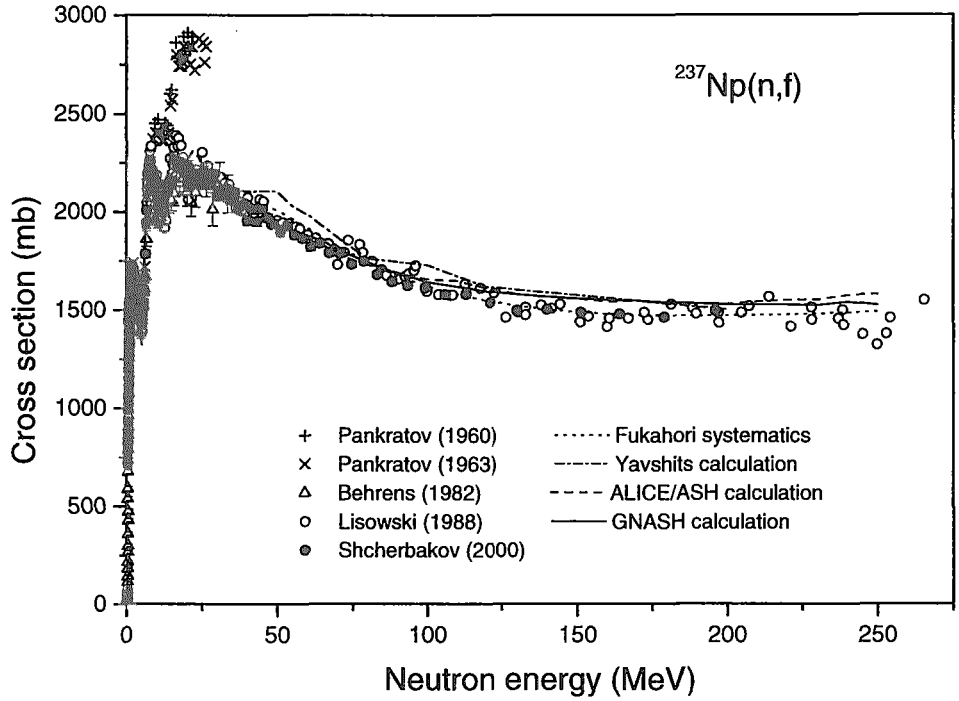

Fig.12 Fission cross section for ^{237}Np calculated with GNASH and ALICE/ASH codes, cross section estimated using the systematics [33], data evaluated in Ref.[34] and measured in Refs.[35-39].

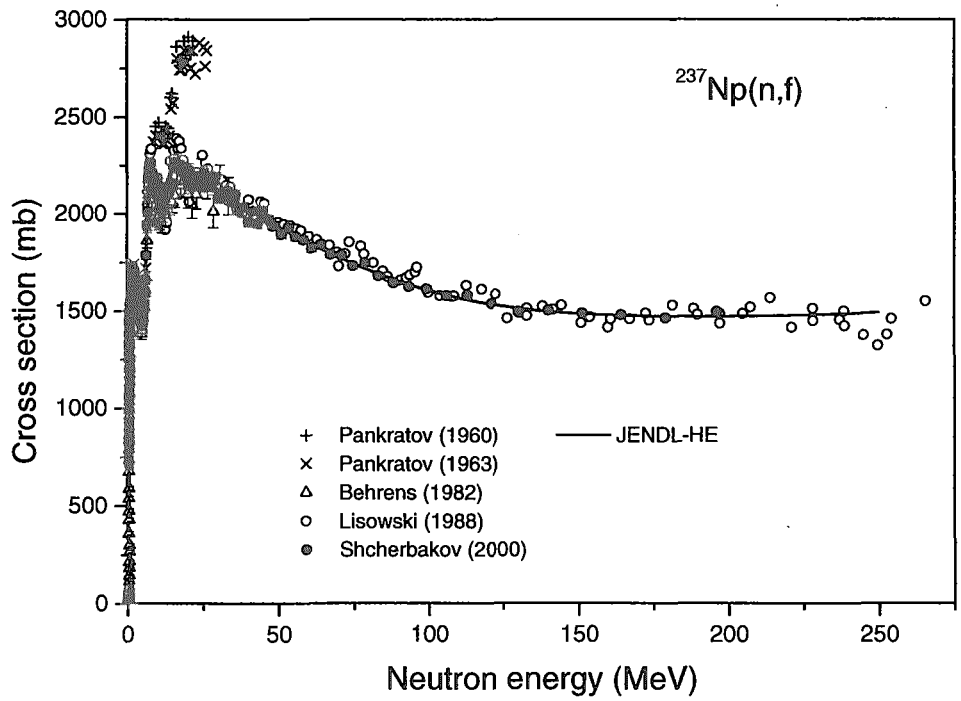

Fig.13 Fission cross section for ^{237}Np at the energies up to 250 MeV evaluated based on the results of calculations and experimental data (solid line) and the experimental data from Refs.[35-39].

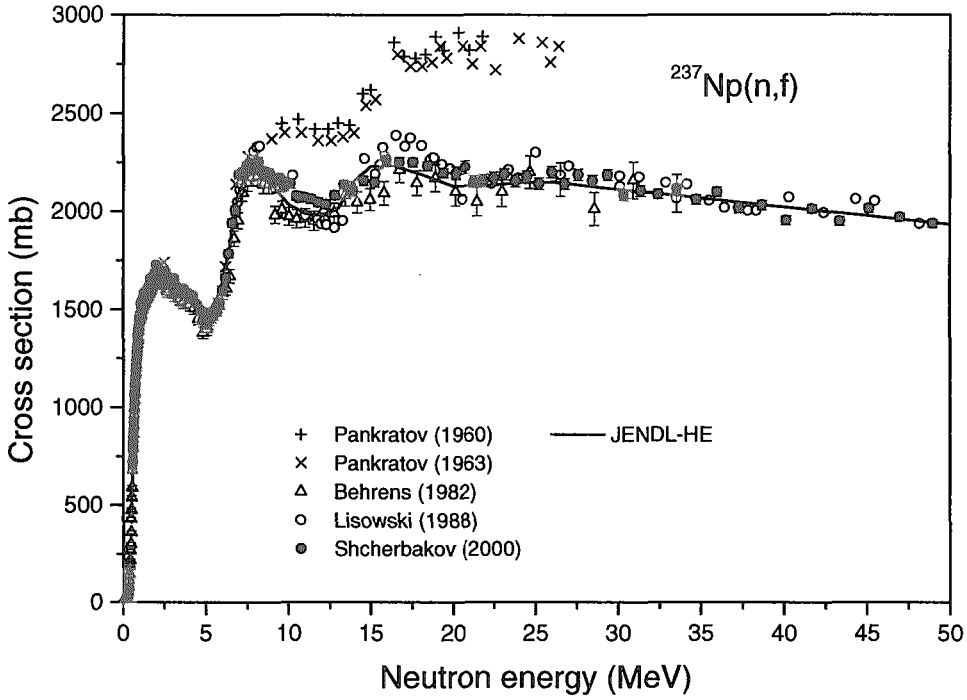

Fig.14 Evaluated fission cross section for ^{237}Np at the energies below 50 MeV. See comments for Fig.13.

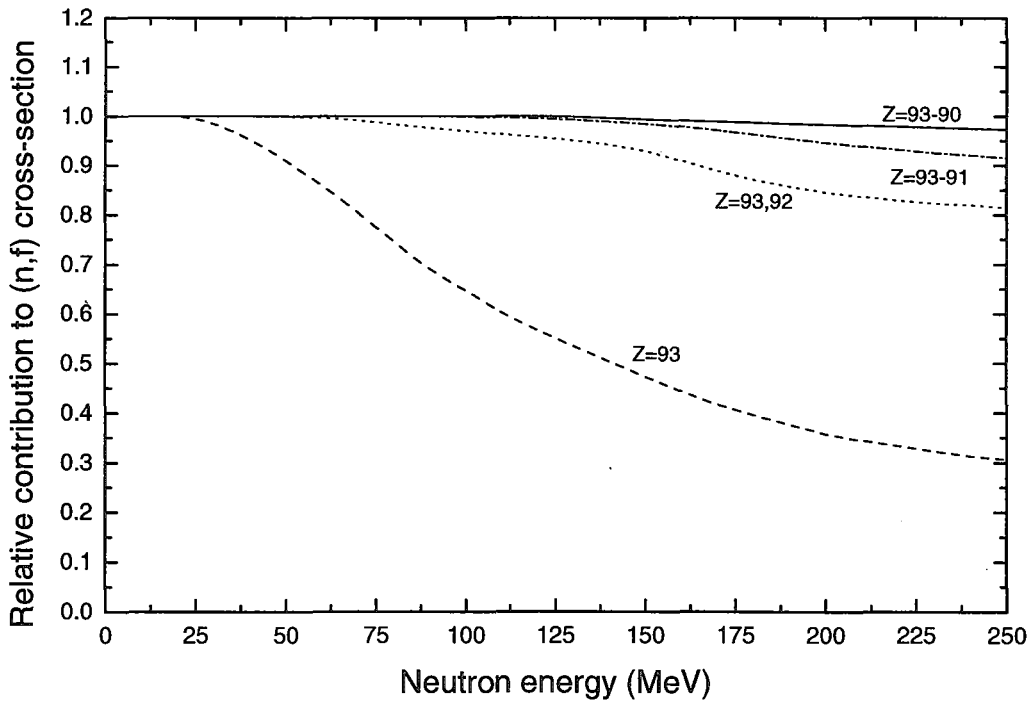

Fig.15 Relative contribution of nuclei with different atomic numbers in total fission cross section for ^{237}Np calculated by GNASH code.

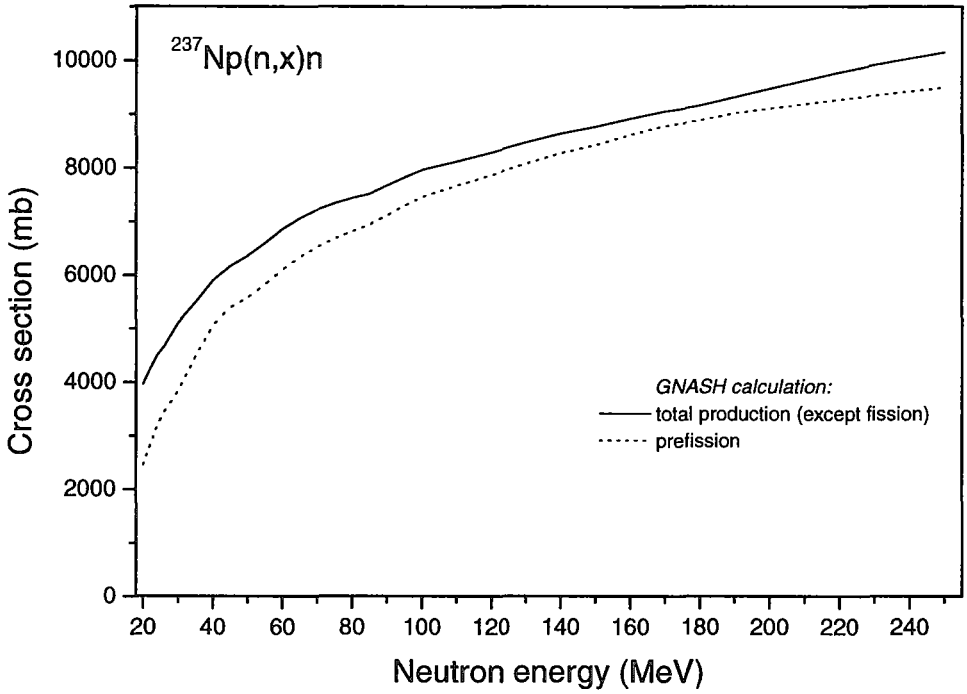

Fig.16 Neutron production cross section for ^{237}Np without contribution from the post-fission evaporation calculated by GNASH code.

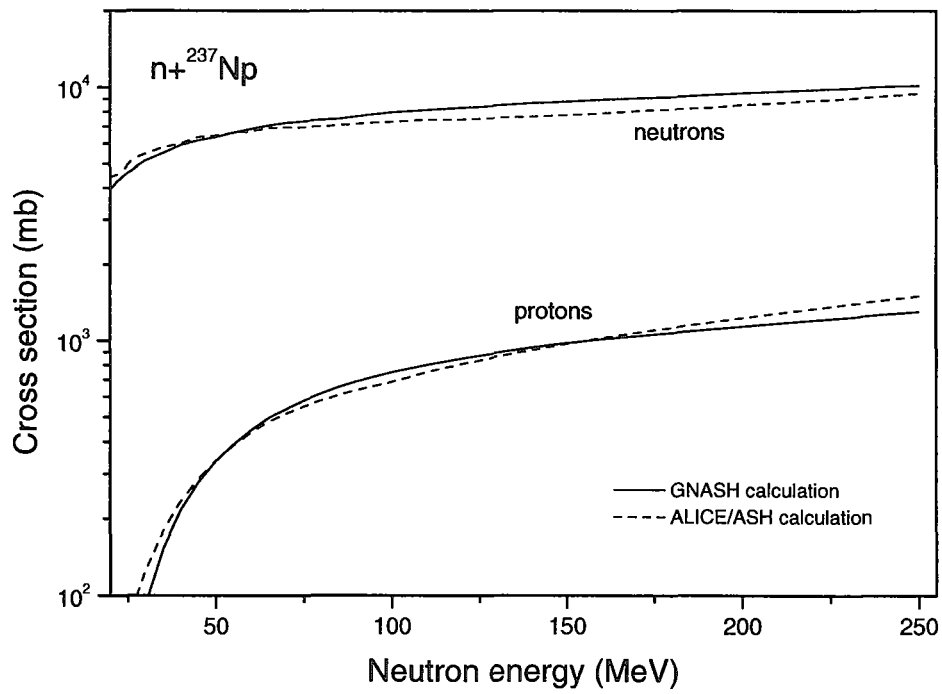

Fig.17 Comparison of neutron and proton production cross sections calculated with GNASH and ALICE/ASH codes for ^{237}Np without contribution from post-fission evaporation.

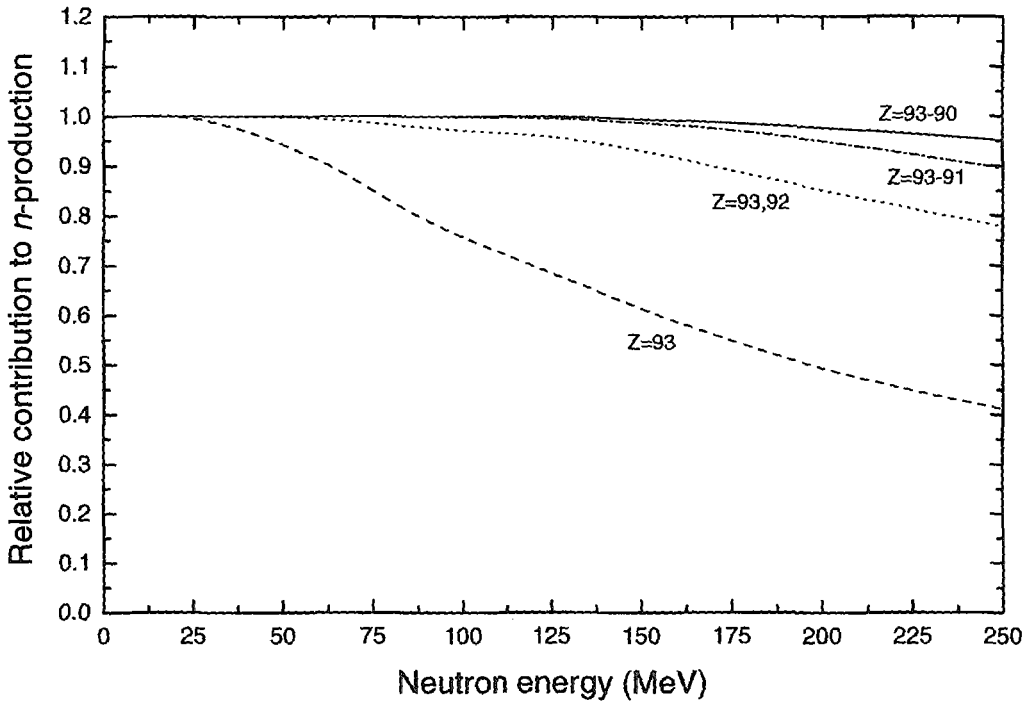

Fig.18 Relative contribution of nuclei with different atomic numbers in the neutron production cross section for ^{237}Np without contribution from post-fission evaporation calculated by GNASH code.

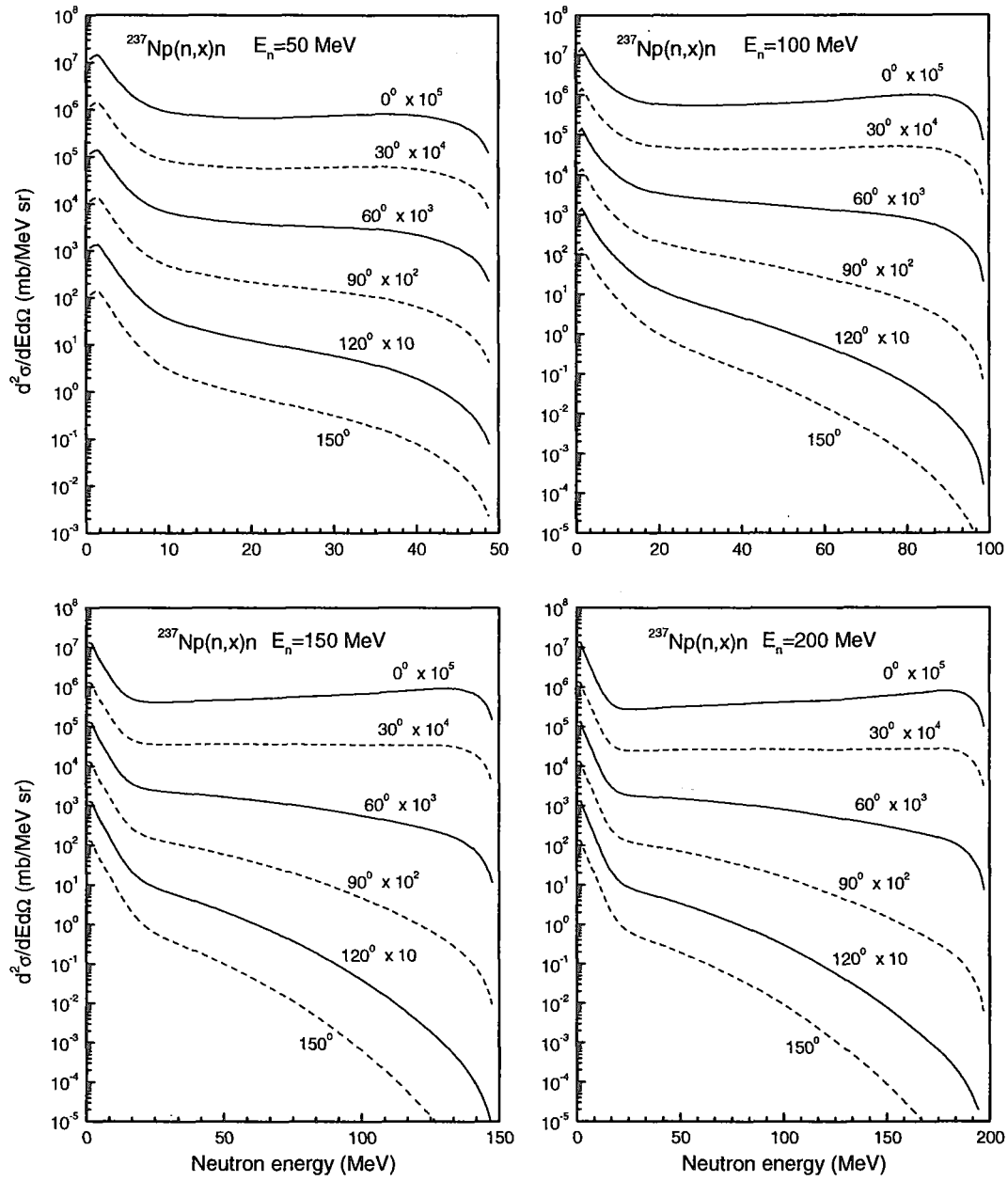

Fig.19 Examples of neutron double-differential cross sections calculated with GNASH code and the Kalbach systematics [13] for ^{237}Np at the incident neutron energy equal to 50, 100, 150 and 200 MeV.

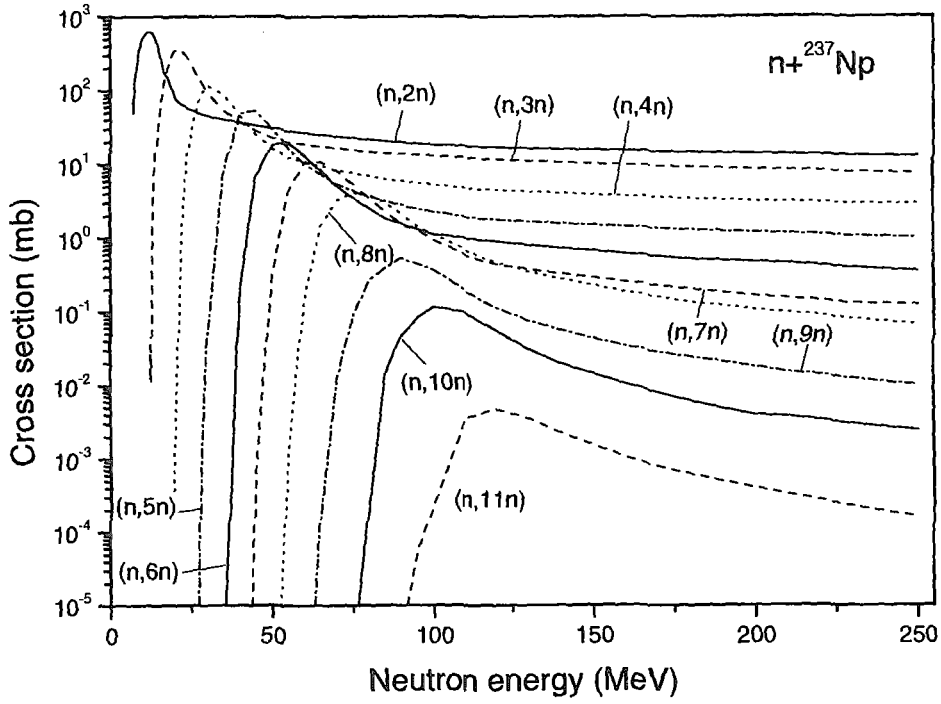

Fig.20 Evaluated (n,xn) reaction cross sections for ^{237}Np.

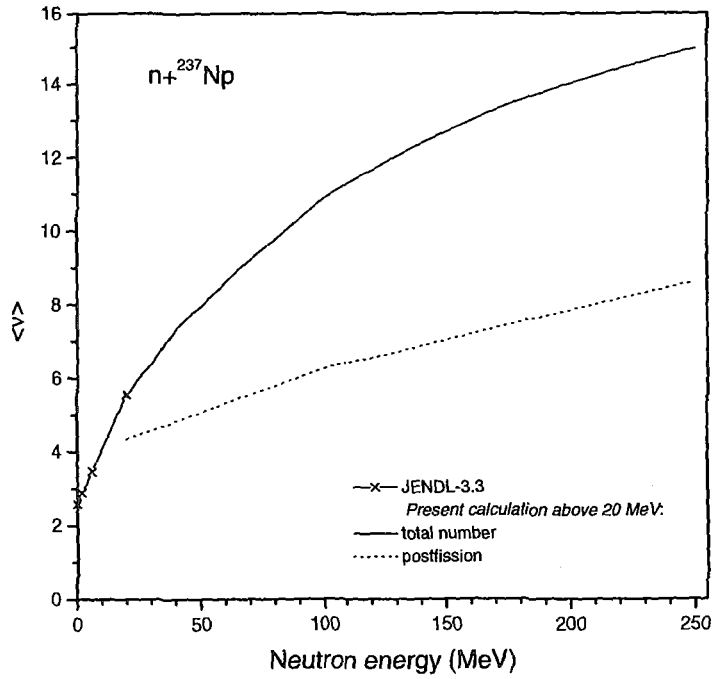

Fig.21 Total number of prompt fission neutrons (solid line) and neutrons emitted from excited fission fragments (dotted line) evaluated in the present work for ^{237}Np. Below 20 MeV JENDL-3.3 data (—x—) are shown.

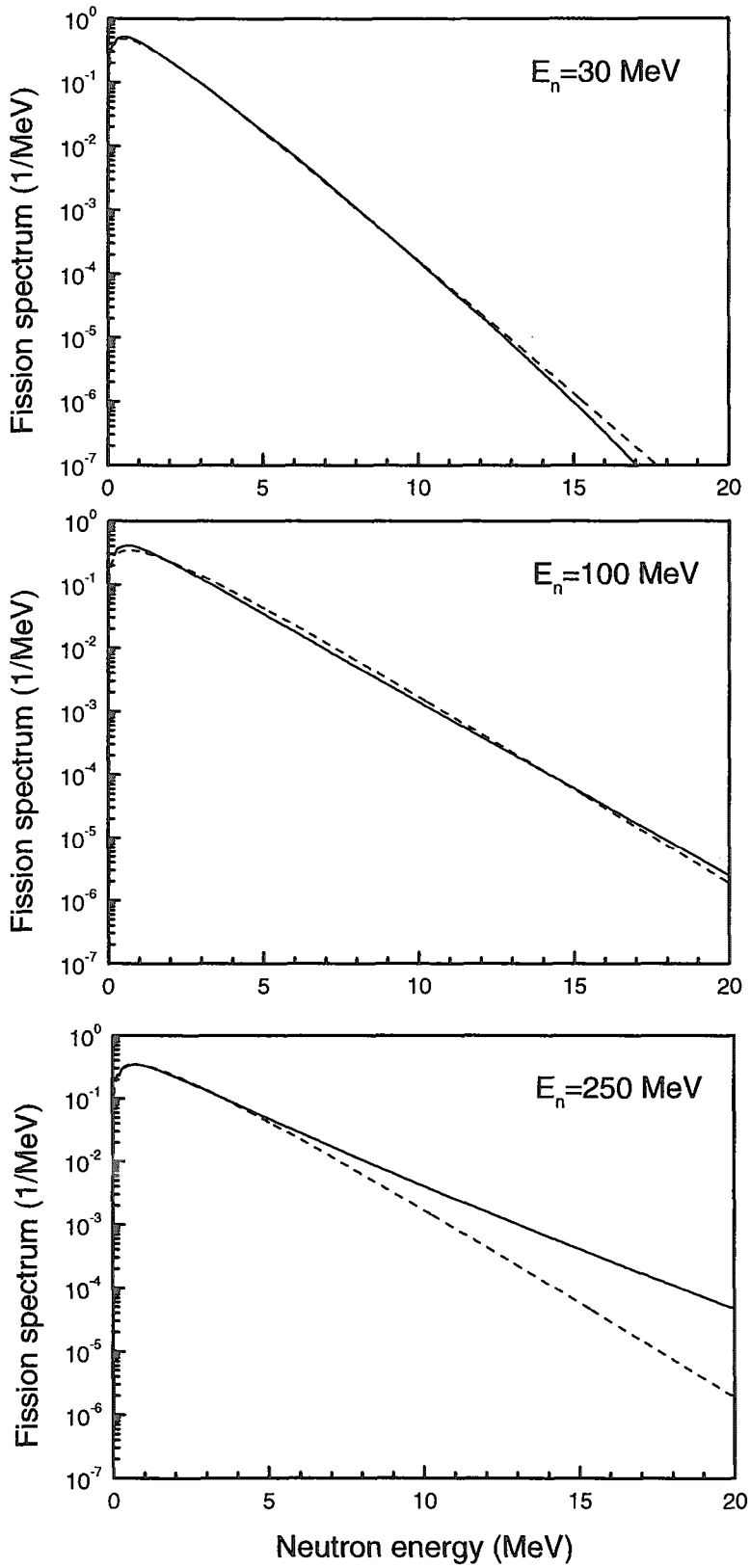

Fig.22 Normalized fission neutron spectra calculated in the present work for ^{237}Np (solid line) and Maxwellian spectra (dashed line) for the primary neutron energies equal to 30, 100 and 250 MeV

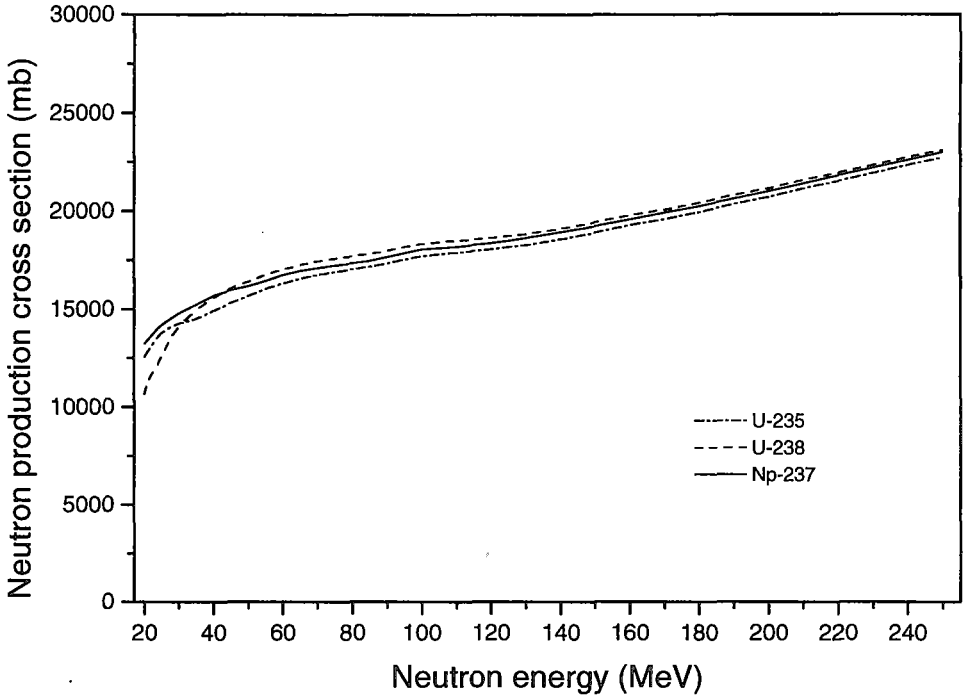

Fig.23 Comparison of total neutron production cross sections including contributions from all processes for uranium isotopes and ^{237}Np.

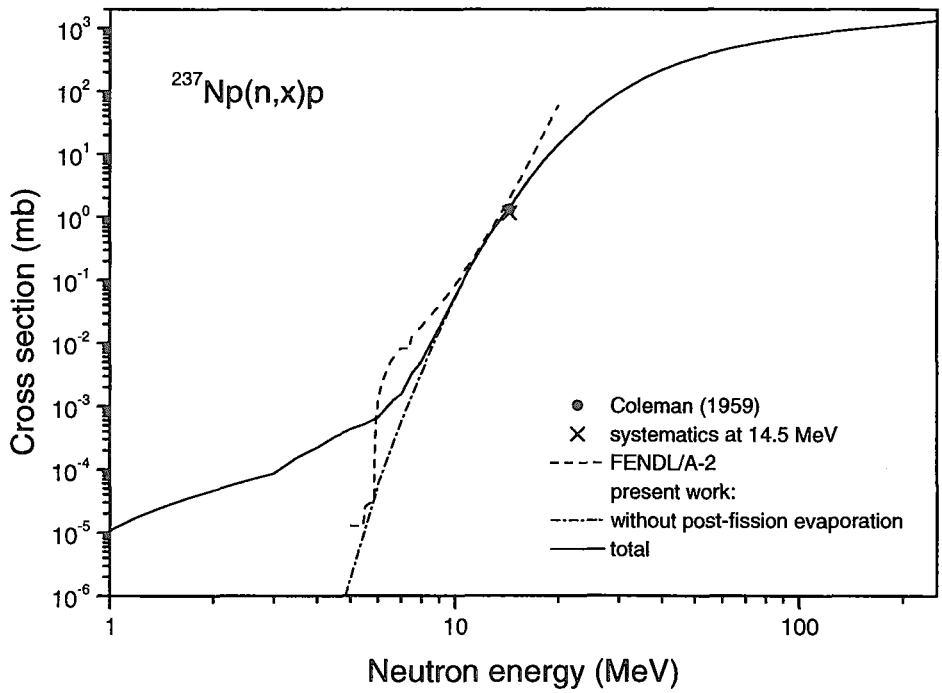

Fig.24 Total proton production cross sections for ^{237}Np, evaluated in the present work, obtained by the systematics [52], measured in Ref.[53] and taken from FENDL/A-2.

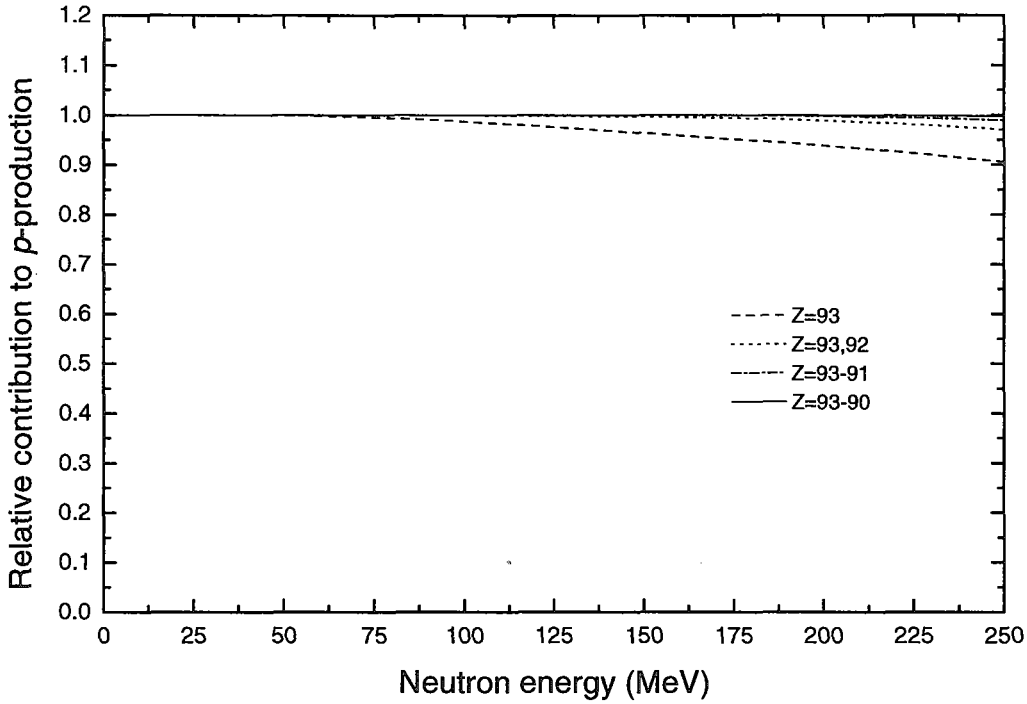

Fig.25 Relative contribution of nuclei with different atomic numbers in the proton production cross section for ^{237}Np without contribution from post-fission evaporation calculated by GNASH code.

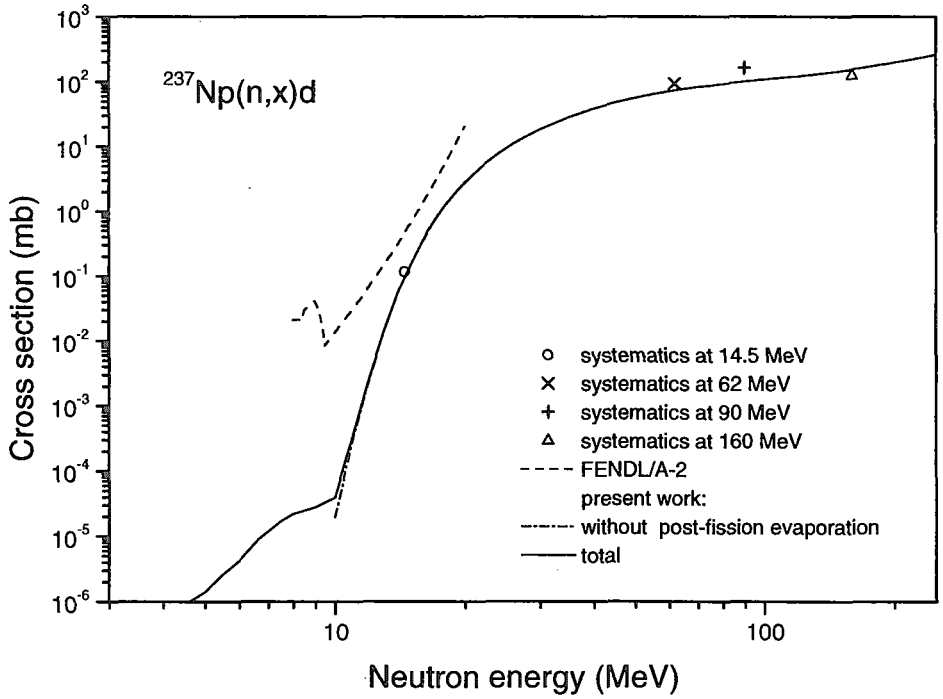

Fig.26 Total deuteron production cross section for ^{237}Np, evaluated in the present work, obtained by systematics and taken from FENDL/A-2.

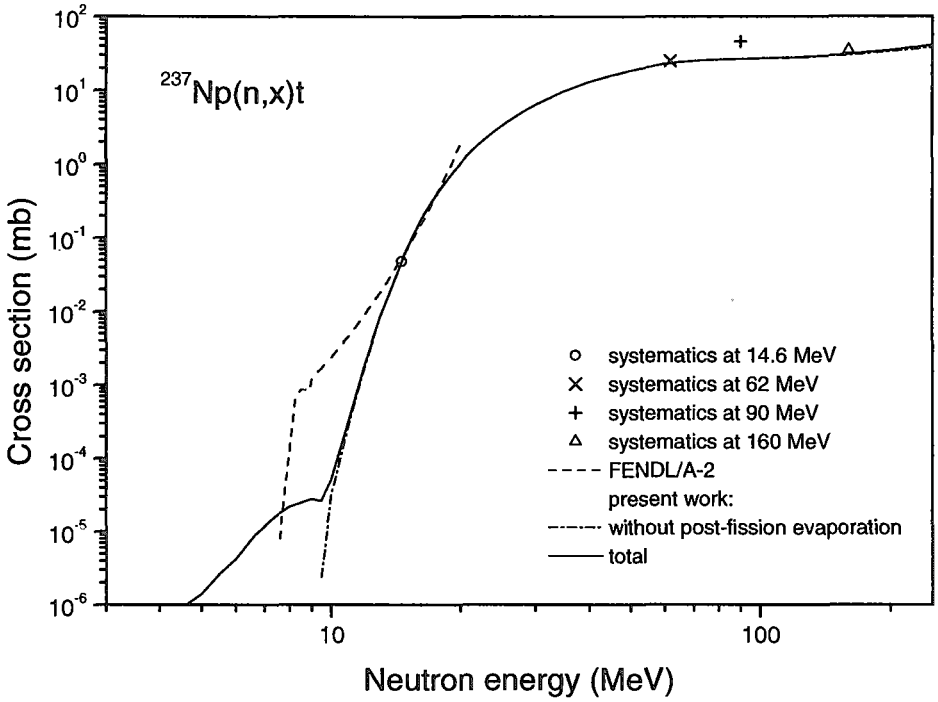

Fig.27 Total triton production cross section for ^{237}Np, evaluated in the present work, obtained by systematics and taken from FENDL/A-2.

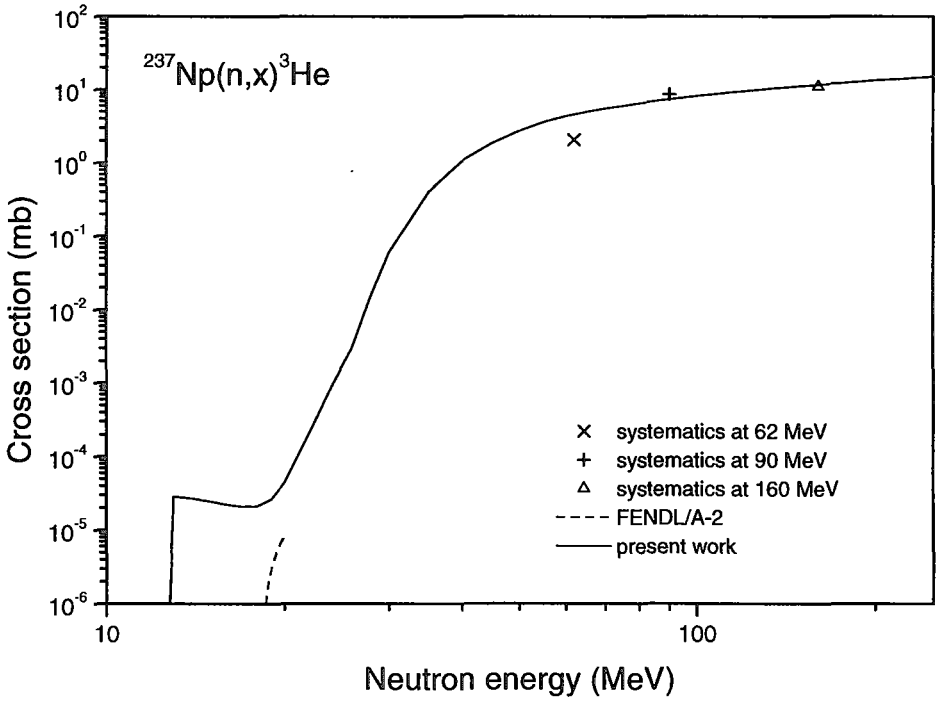

Fig.28 Total ^{3}He-production cross section for ^{237}Np, evaluated in the present work, obtained by systematics and taken from FENDL/A-2

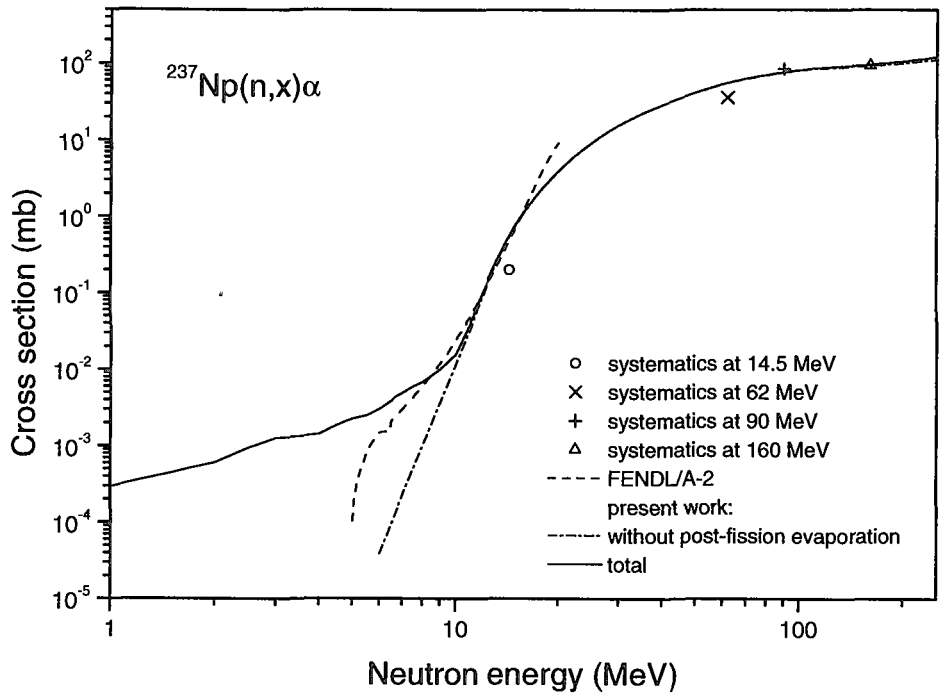

Fig.29 Total α-production cross section for ^{237}Np, evaluated in the present work, obtained by systematics and taken from FENDL/A-2.

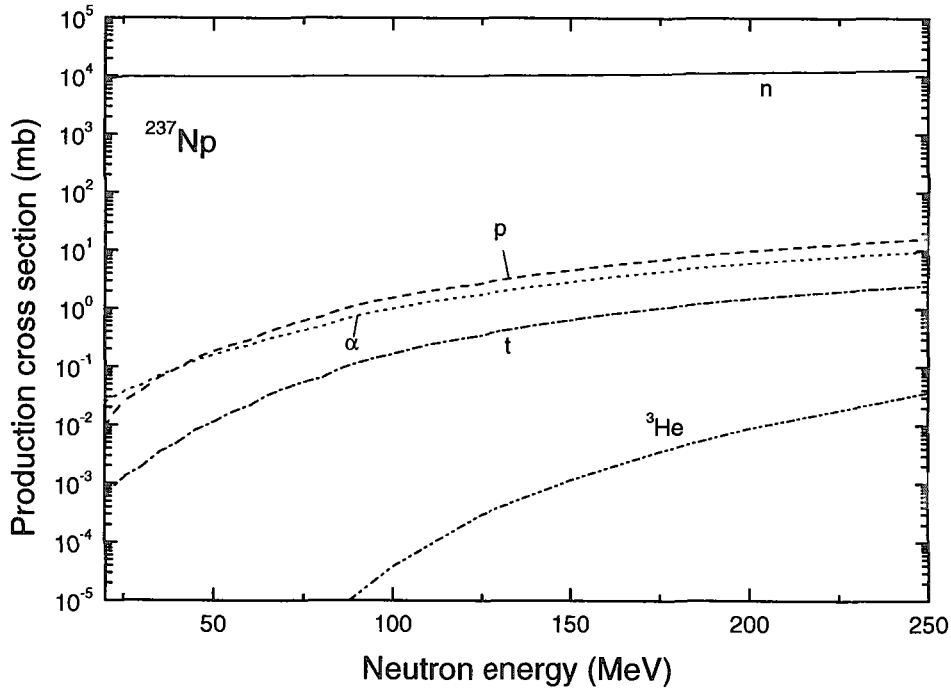

Fig.30 Production cross section for different particles emitted from fission fragments calculated in the present work.

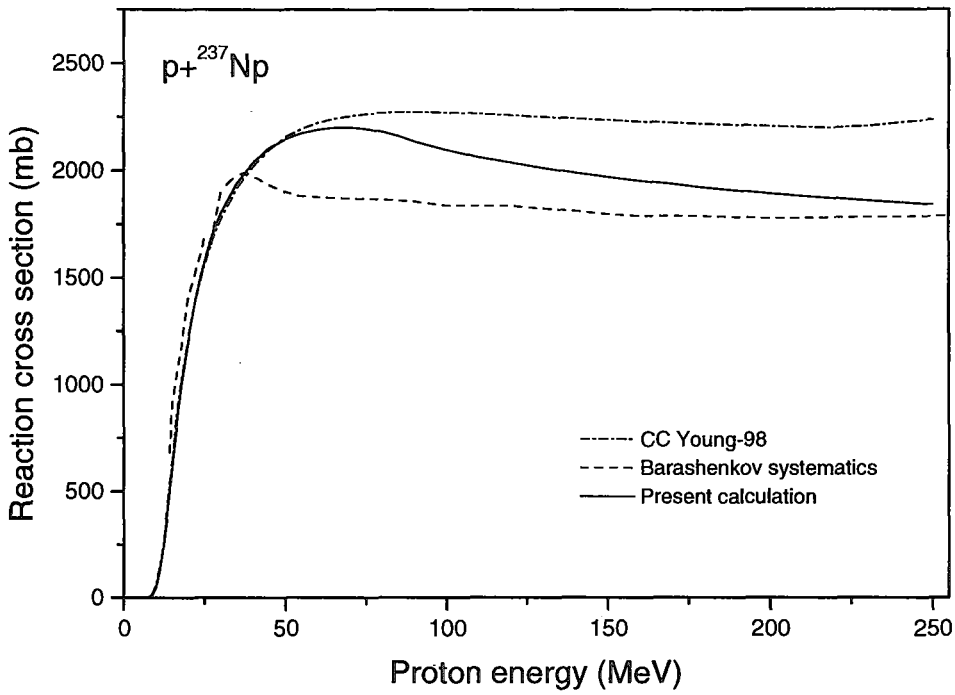

Fig.31 Proton reaction cross section for ^{237}Np calculated using different sets of coupled-channel optical model parameters and evaluated according to Ref.[32].

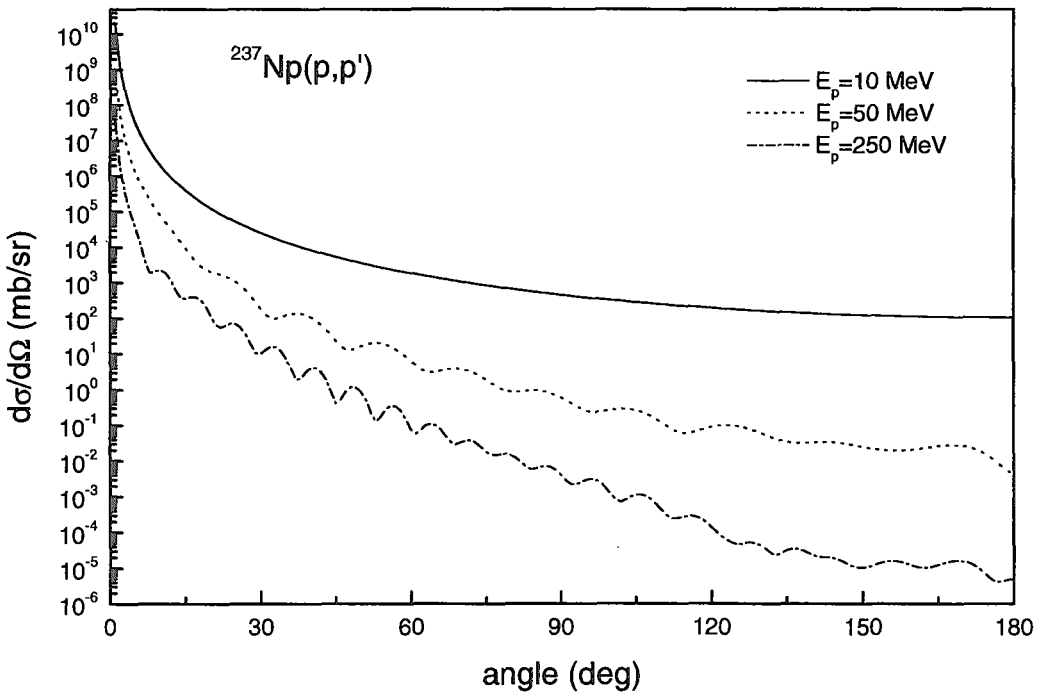

Fig.32 Proton elastic scattering angular distributions calculated in the present work for ^{237}Np at the different primary proton energies.

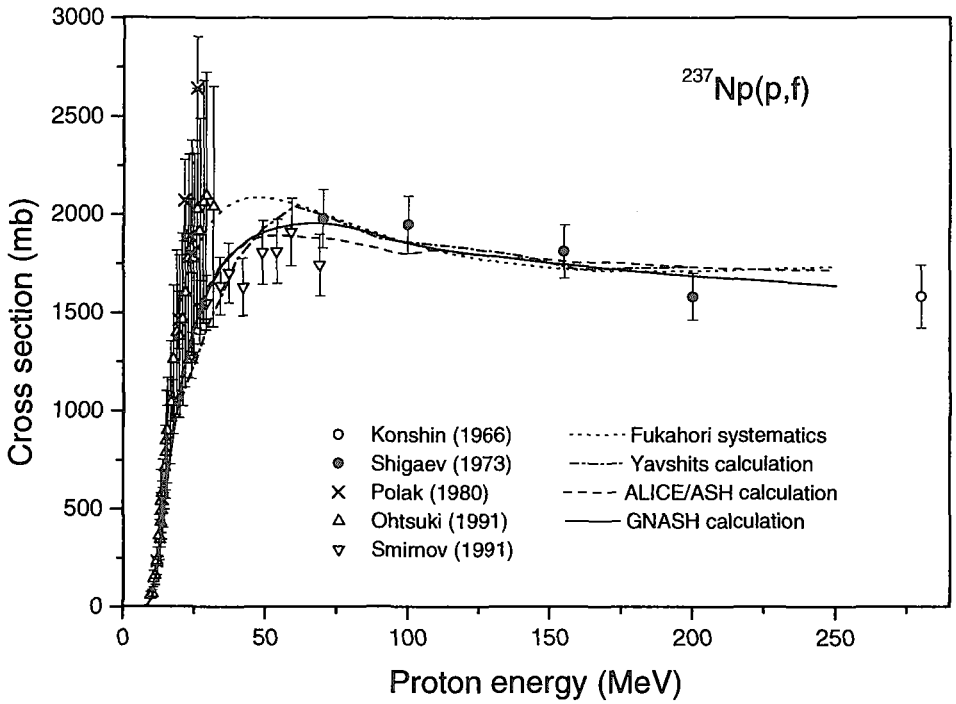

Fig.33 Fission cross section for p+^{237}Np interaction calculated with GNASH and ALICE/ASH codes, cross section estimated by the systematics [33], data evaluated in Ref.[34] and measured in Refs.[40-44].

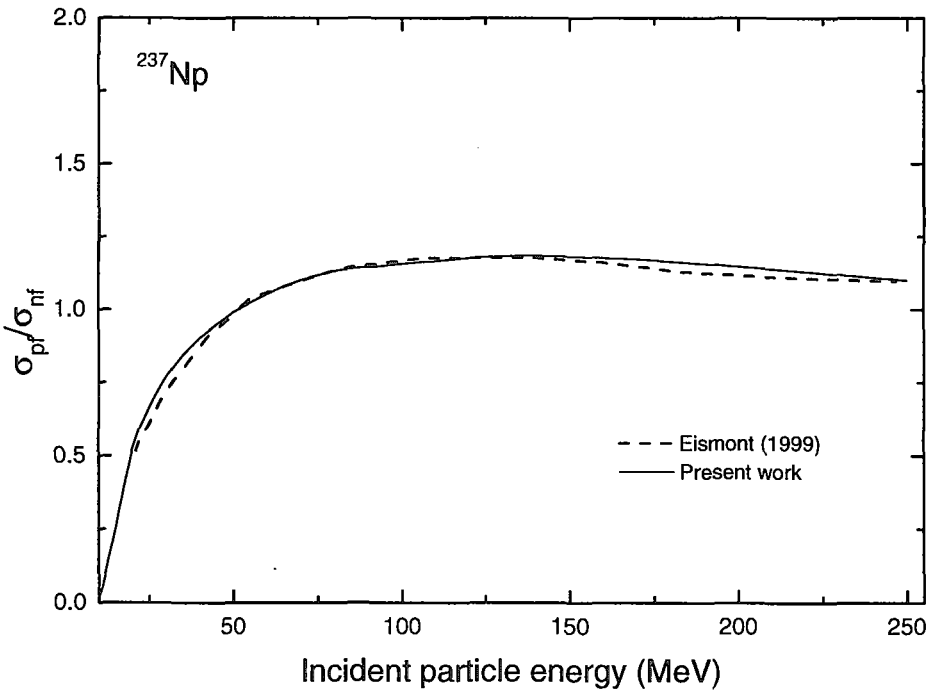

Fig.34 Ratio of (p,f) and (n,f) cross sections for ^{237}Np obtained in the present work (solid line) and in Ref.[46] (dashed line).

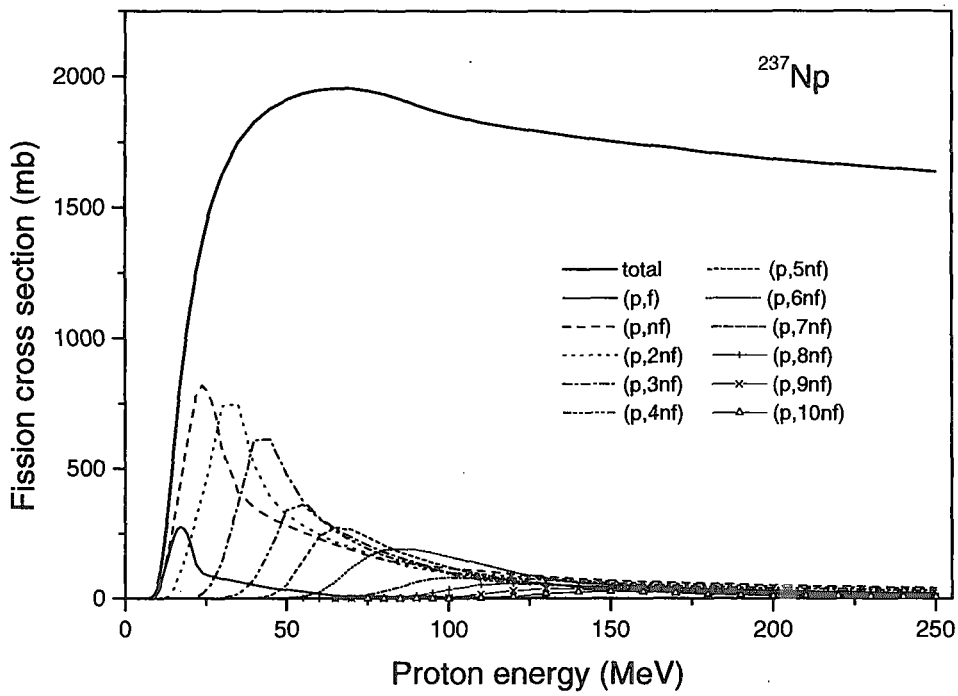

Fig.35 (p,f) reaction cross section and contribution of (p,xnf) reactions calculated in the present work for ^{237}Np.

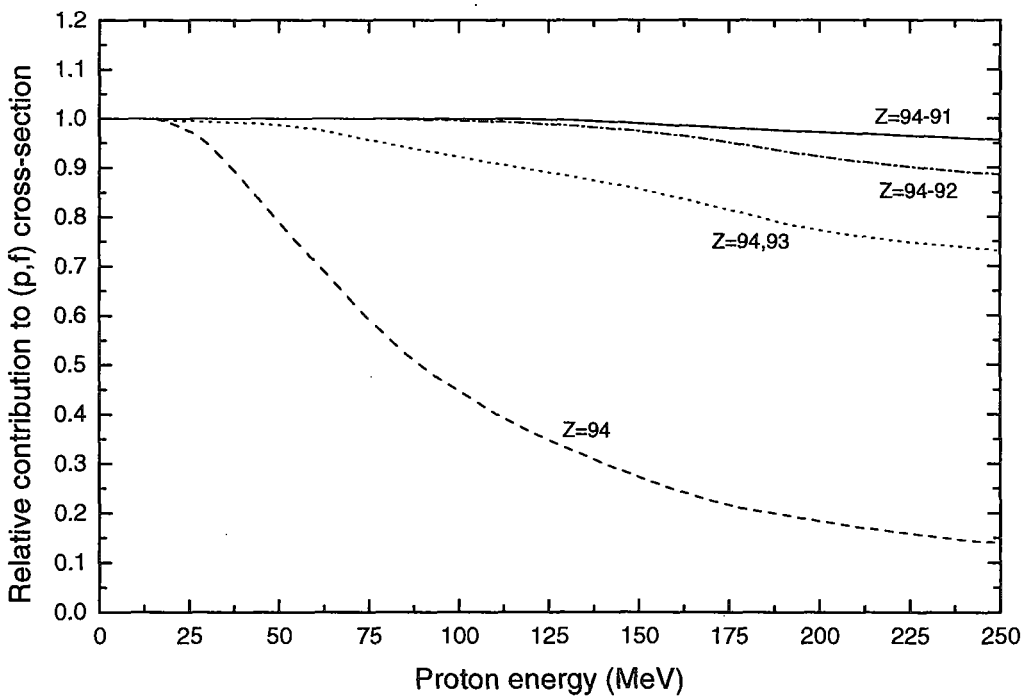

Fig.36 Relative contribution of nuclei with different atomic numbers in total fission cross section for ^{2379}Np irradiated by protons calculated in the present work.

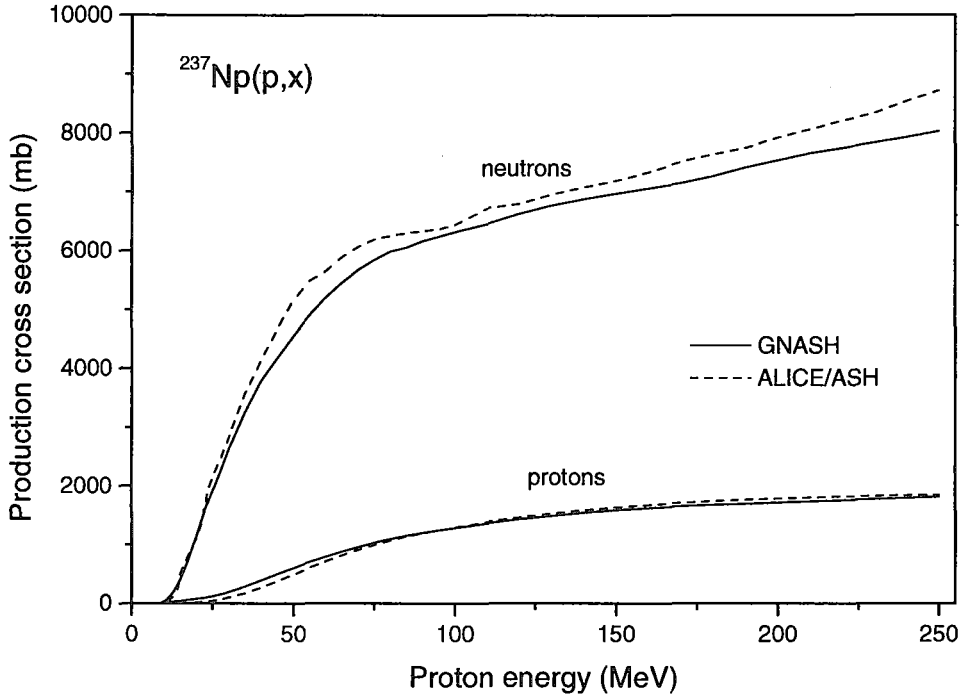

Fig.37 Neutron and proton production cross sections calculated with GNASH and ALICE/ASH codes without post-fission evaporation contribution for proton induced reactions p+^{237}Np.

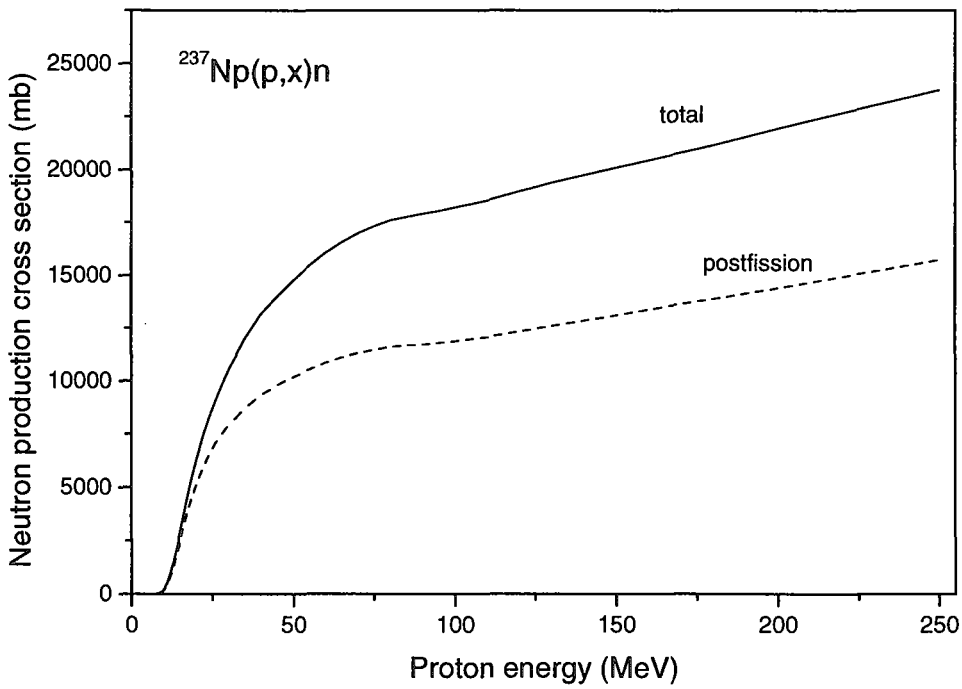

Fig.38 Total neutron production cross section for ^{237}Np including contribution from (p,xnypzα) reactions, pre- and post-fission events (solid line), the part of this cross section corresponding to the post-fission evaporation (dashed line).

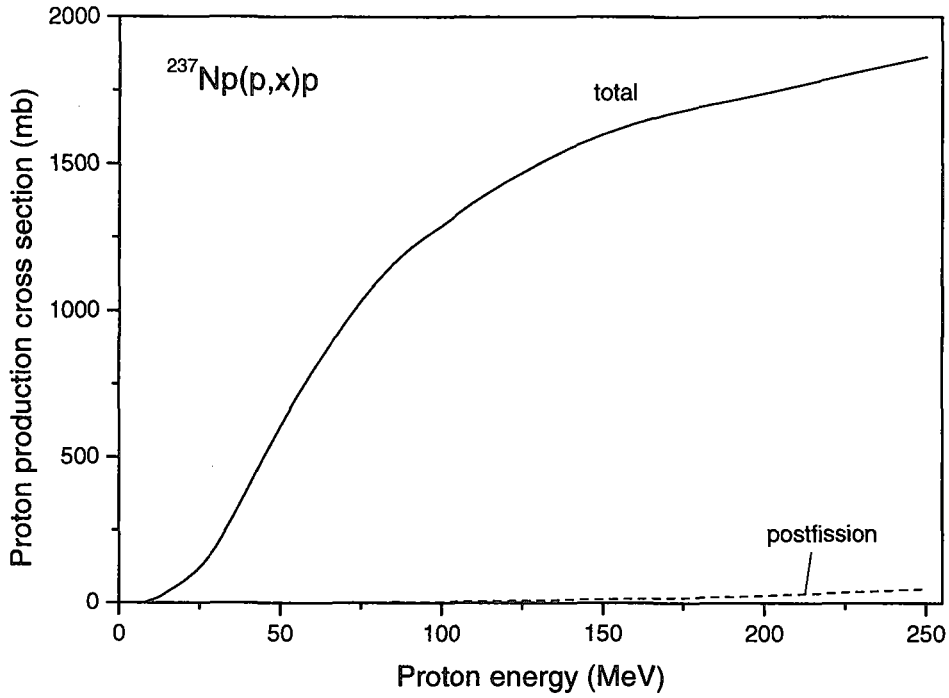

Fig.39 Total proton production cross section for ^{237}Np including contribution from (p,xnypzα) reactions, pre- and post-fission events (solid line), the part of this cross section corresponding to the post-fission evaporation (dashed line).

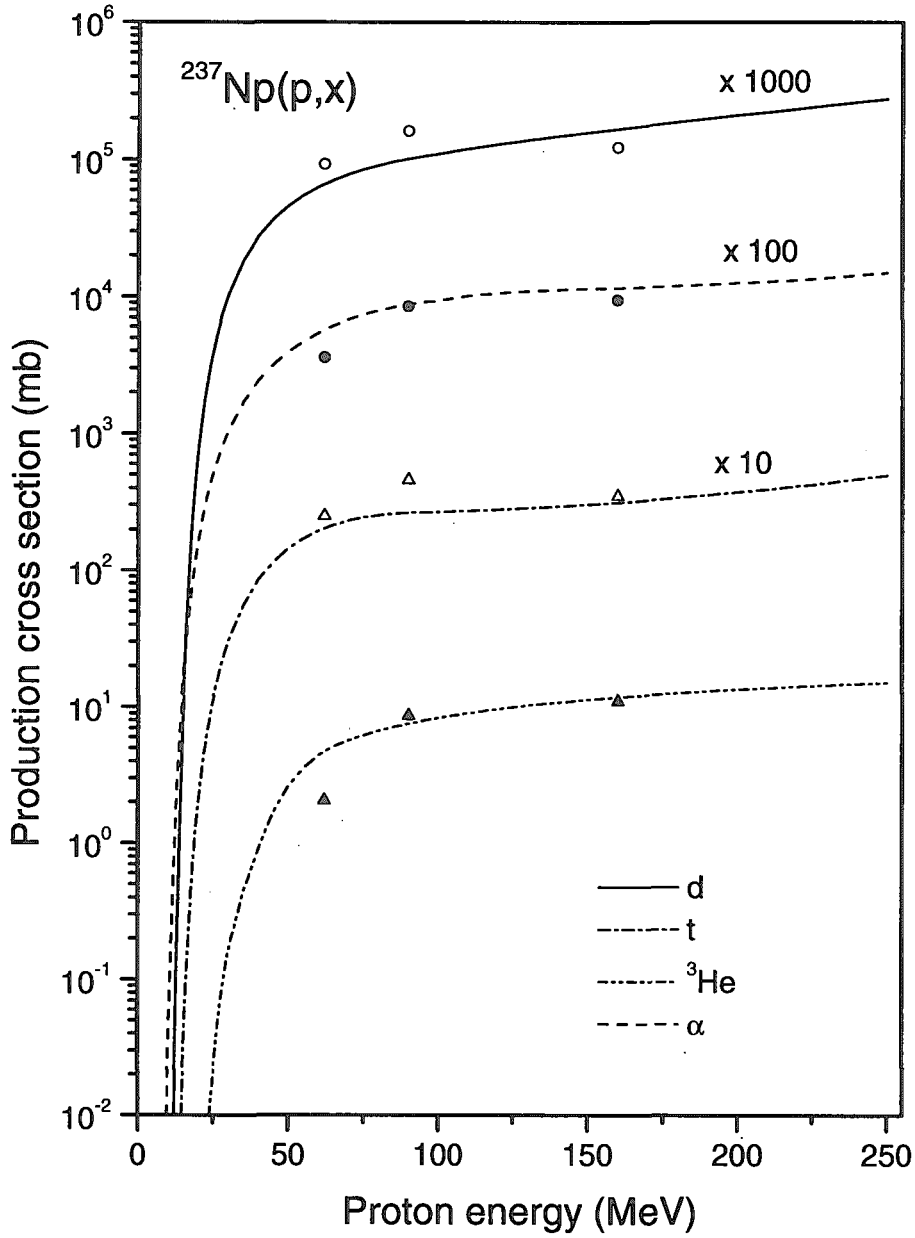

Fig.40 Total deuteron-, triton-, ^{3}He- and α-production cross sections for ^{237}Np irradiated by protons

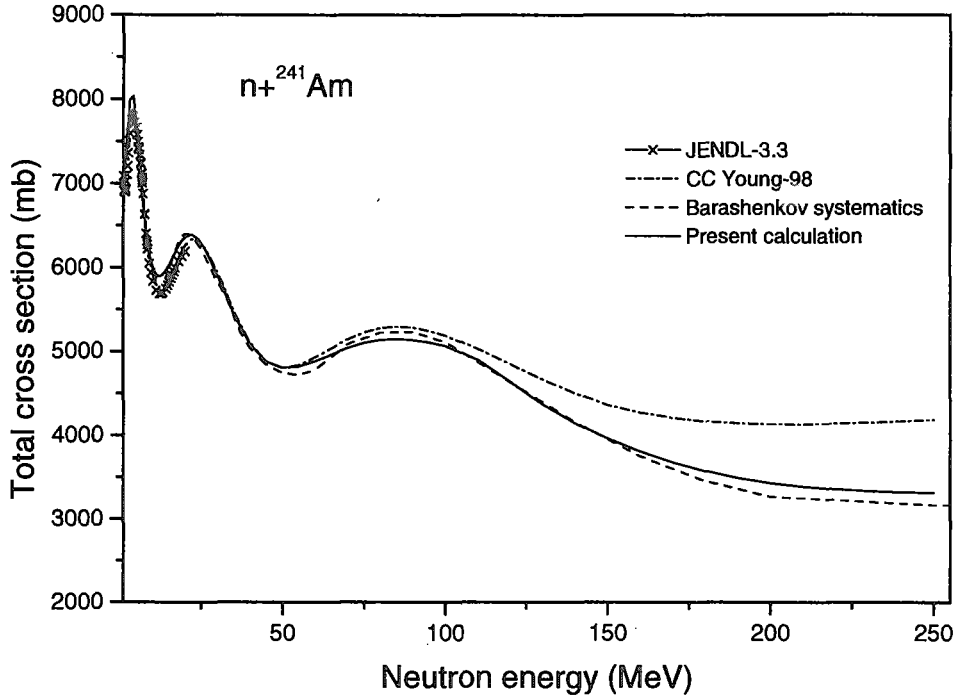

Fig.41 Neutron total cross section for ^{241}Am calculated with coupled-channel optical model, estimated by the systematics [32,48] and taken from JENDL-3.3.

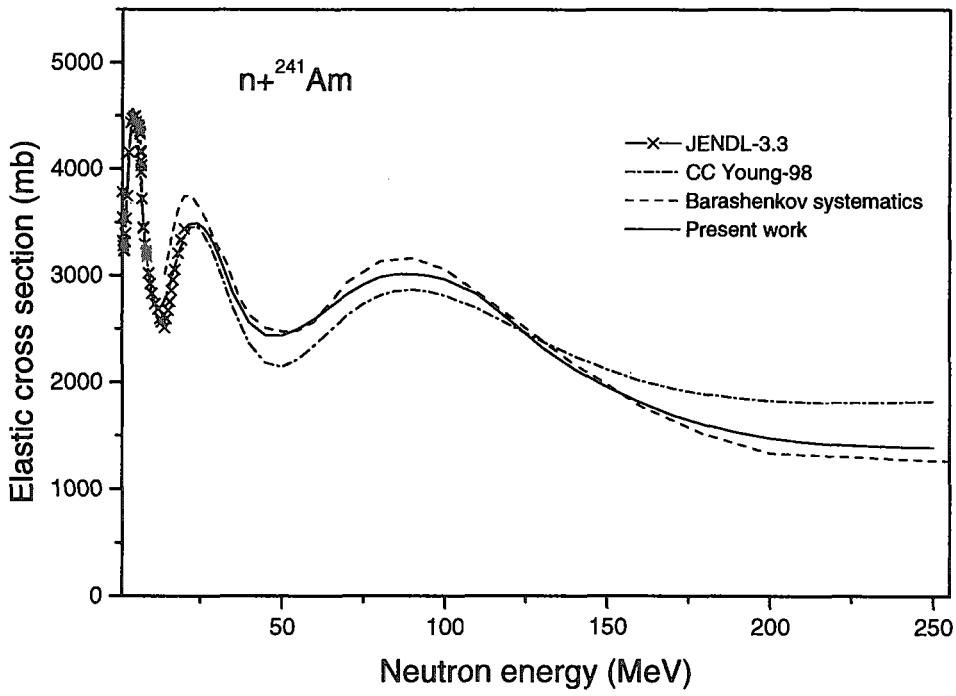

Fig.42 Neutron elastic scattering cross section for ^{241}Am calculated with coupled-channel optical model, estimated by the systematics [32,48] and taken from JENDL-3.3.

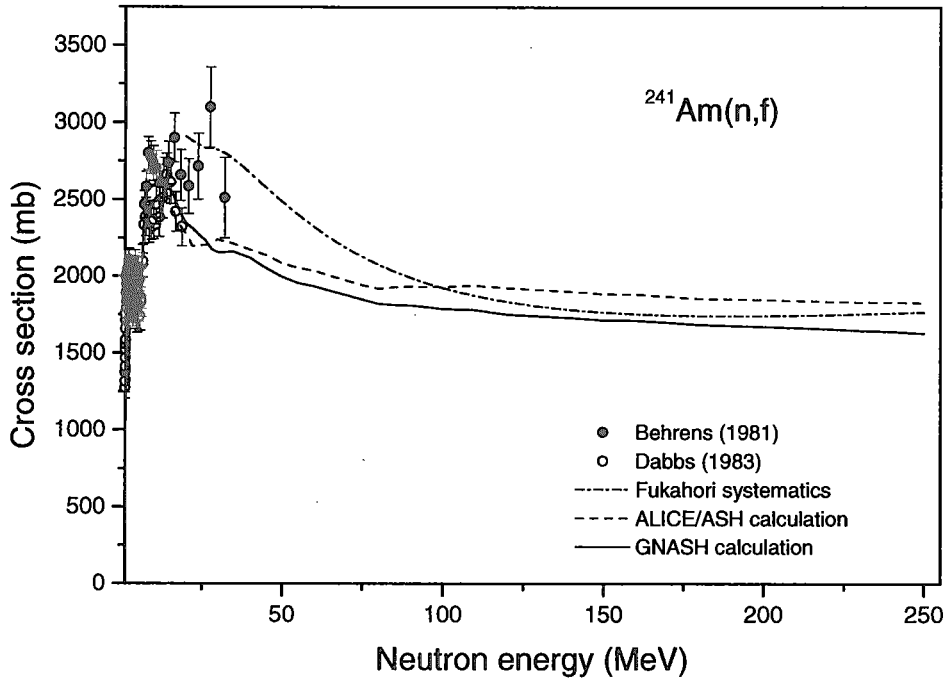

Fig.43 Neutron induced fission cross section for ^{241}Am calculated with GNASH and ALICE/ASH codes, cross section estimated by the systematics [33] and measured in Refs.[49,50].

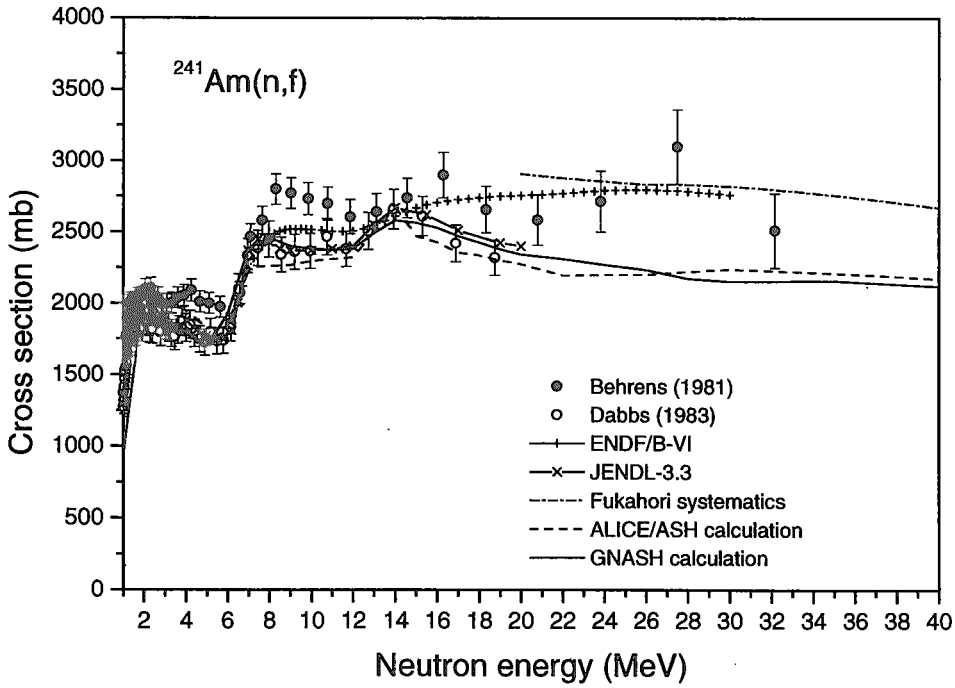

Fig.44 Neutron induced fission cross section for ^{241}Am calculated with GNASH and ALICE/ASH codes, cross section estimated by the systematics [33], measured in Refs.[49,50] and taken from JENDL-3.3 and ENDF/B-VI.

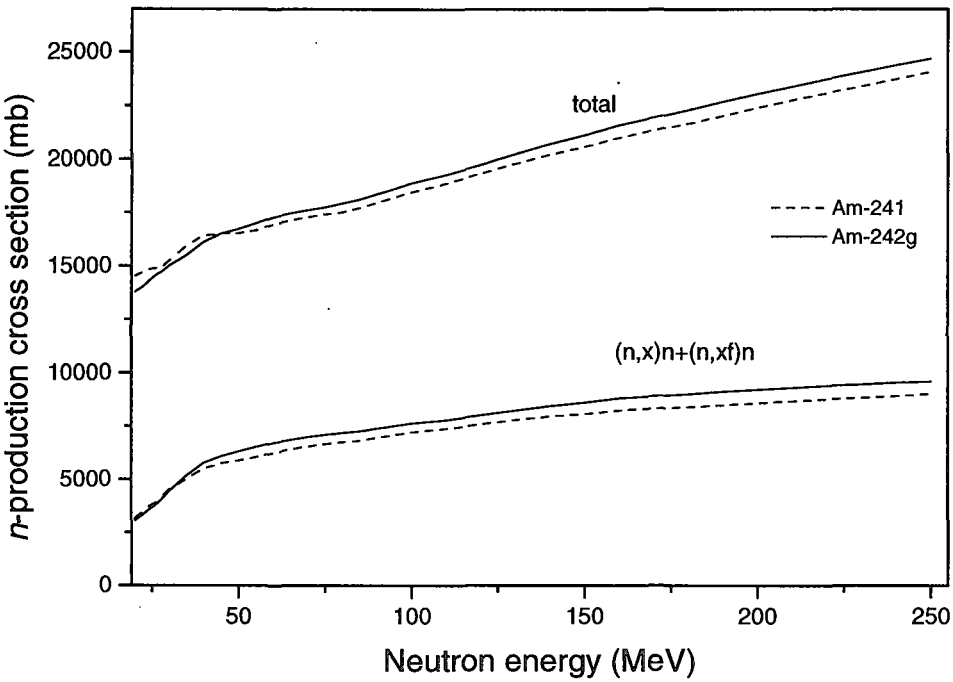

Fig.45 Neutron production cross section for ^{241}Am and ^{242g}Am.

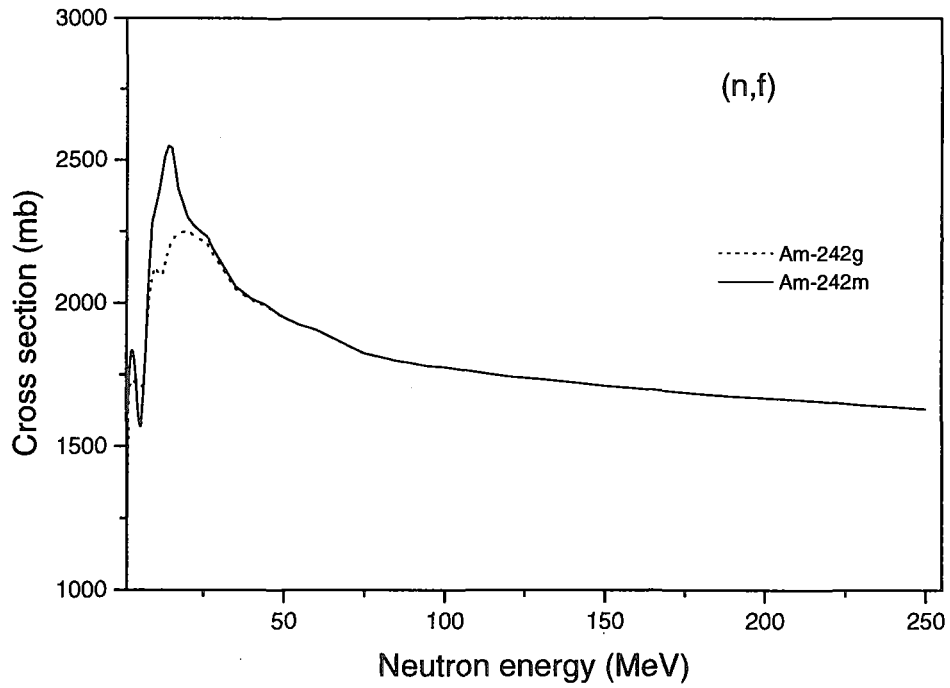

Fig.46 Recommended neutron induced fission cross section for ^{242g}Am and ^{242m}Am.

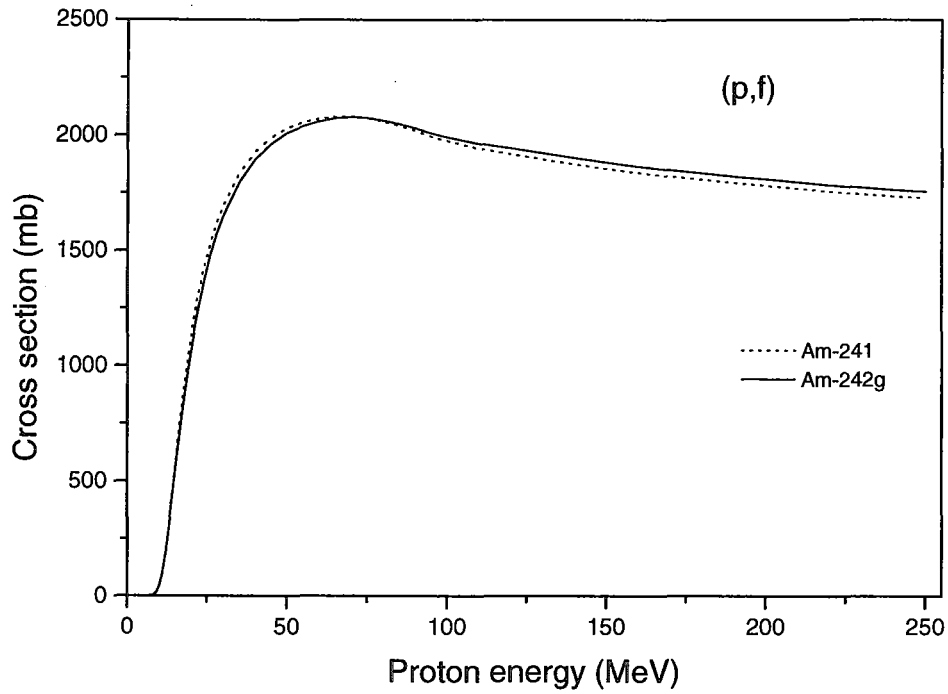

Fig.47 Recommended proton induced fission cross section for ^{241}Am and ^{242g}Am.

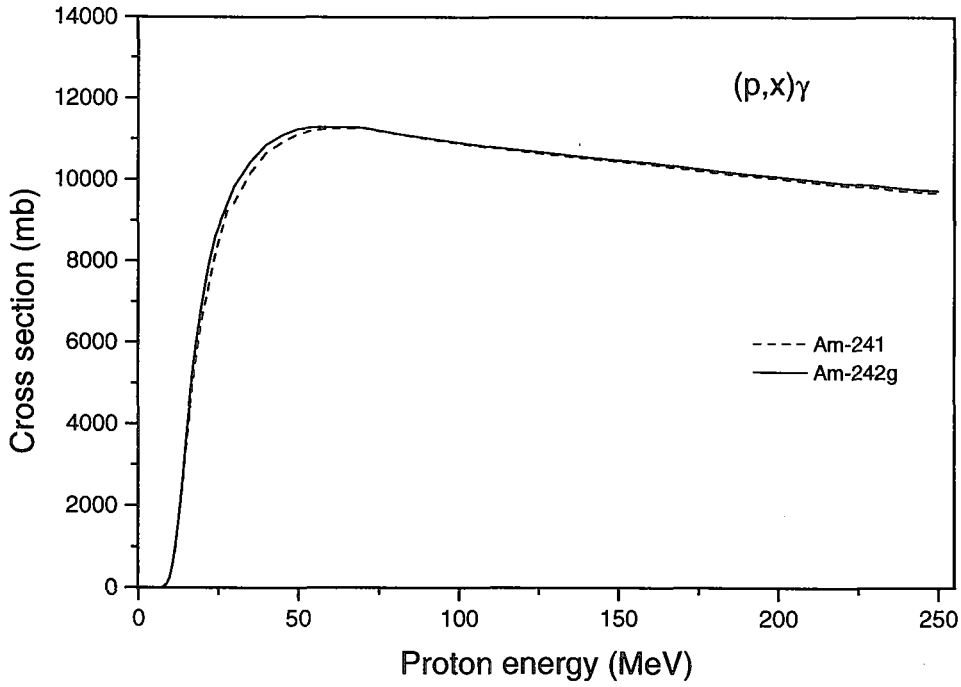

Fig.48 Evaluated γ-production cross section for p+ ^{241}Am and p+^{242g}Am interactions.

国際単位系 (SI) と換算表

表1　SI基本単位および補助単位

量	名称	記号
長さ	メートル	m
質量	キログラム	kg
時間	秒	s
電流	アンペア	A
熱力学温度	ケルビン	K
物質量	モル	mol
光度	カンデラ	cd
平面角	ラジアン	rad
立体角	ステラジアン	sr

表2　SIと併用される単位

名称	記号
分，時，日	min，h，d
度，分，秒	°，′，″
リットル	l，L
トン	t
電子ボルト	eV
原子質量単位	u

1 eV=1.60218×10^{-19} J

1 u=1.66054×10^{-27} kg

表3　固有の名称をもつSI組立単位

量	名称	記号	他のSI単位による表現
周波数	ヘルツ	Hz	s^{-1}
力	ニュートン	N	m·kg/s^2
圧力，応力	パスカル	Pa	N/m^2
エネルギー，仕事，熱量	ジュール	J	N·m
工率，放射束	ワット	W	J/s
電気量，電荷	クーロン	C	A·s
電位，電圧，起電力	ボルト	V	W/A
静電容量	ファラド	F	C/V
電気抵抗	オーム	Ω	V/A
コンダクタンス	ジーメンス	S	A/V
磁束	ウェーバ	Wb	V·s
磁束密度	テスラ	T	Wb/m^2
インダクタンス	ヘンリー	H	Wb/A
セルシウス温度	セルシウス度	℃	
光束	ルーメン	lm	cd·sr
照度	ルクス	lx	lm/m^2
放射能	ベクレル	Bq	s^{-1}
吸収線量	グレイ	Gy	J/kg
線量当量	シーベルト	Sv	J/kg

表4　SIと共に暫定的に維持される単位

名称	記号
オングストローム	Å
バーン	b
バール	bar
ガル	Gal
キュリー	Ci
レントゲン	R
ラド	rad
レム	rem

1 Å=0.1 nm=10^{-10} m

1 b=100 fm^2=10^{-28} m^2

1 bar=0.1 MPa=10^5 Pa

1 Gal=1 cm/s^2=10^{-2} m/s^2

1 Ci=3.7×10^{10} Bq

1 R=2.58×10^{-4} C/kg

1 rad=1 cGy=10^{-2} Gy

1 rem=1 cSv=10^{-2} Sv

表5　SI接頭語

倍数	接頭語	記号
10^{18}	エクサ	E
10^{15}	ペタ	P
10^{12}	テラ	T
10^{9}	ギガ	G
10^{6}	メガ	M
10^{3}	キロ	k
10^{2}	ヘクト	h
10^{1}	デカ	da
10^{-1}	デシ	d
10^{-2}	センチ	c
10^{-3}	ミリ	m
10^{-6}	マイクロ	μ
10^{-9}	ナノ	n
10^{-12}	ピコ	p
10^{-15}	フェムト	f
10^{-18}	アト	a

（注）

1. 表1－5は「国際単位系」第5版，国際度量衡局 1985年刊行による。ただし，1 eVおよび1 uの値はCODATAの1986年推奨値によった。
2. 表4には海里，ノット，アール，ヘクタールも含まれているが日常の単位なのでここでは省略した。
3. barは，JISでは流体の圧力を表わす場合に限り表2のカテゴリーに分類されている。
4. EC閣僚理事会指令ではbar，barnおよび「血圧の単位」mmHgを表2のカテゴリーに入れている。

換算表

力	N(=10^5 dyn)	kgf	lbf
	1	0.101972	0.224809
	9.80665	1	2.20462
	4.44822	0.453592	1

粘度　1 Pa·s(N·s/m^2)=10 P(ポアズ)(g/(cm·s))

動粘度　1 m^2/s=10^4 St(ストークス)(cm^2/s)

圧力	MPa(=10 bar)	kgf/cm^2	atm	mmHg(Torr)	lbf/in^2(psi)
	1	10.1972	9.86923	7.50062×10^3	145.038
	0.0980665	1	0.967841	735.559	14.2233
	0.101325	1.03323	1	760	14.6959
	1.33322×10^{-4}	1.35951×10^{-3}	1.31579×10^{-3}	1	1.93368×10^{-2}
	6.89476×10^{-3}	7.03070×10^{-2}	6.80460×10^{-2}	51.7149	1

エネルギー・仕事・熱量	J(=10^7 erg)	kgf·m	kW·h	cal(計量法)	Btu	ft·lbf	eV
	1	0.101972	2.77778×10^{-7}	0.238889	9.47813×10^{-4}	0.737562	6.24150×10^{18}
	9.80665	1	2.72407×10^{-6}	2.34270	9.29487×10^{-3}	7.23301	6.12082×10^{19}
	3.6×10^6	3.67098×10^5	1	8.59999×10^5	3412.13	2.65522×10^6	2.24694×10^{25}
	4.18605	0.426858	1.16279×10^{-6}	1	3.96759×10^{-3}	3.08747	2.61272×10^{19}
	1055.06	107.586	2.93072×10^{-4}	252.042	1	778.172	6.58515×10^{21}
	1.35582	0.138255	3.76616×10^{-7}	0.323890	1.28506×10^{-3}	1	8.46233×10^{18}
	1.60218×10^{-19}	1.63377×10^{-20}	4.45050×10^{-26}	3.82743×10^{-20}	1.51857×10^{-22}	1.18171×10^{-19}	1

1 cal=4.18605 J(計量法)

=4.184 J　(熱化学)

=4.1855 J　(15 °C)

=4.1868 J(国際蒸気表)

仕事率　1 PS(仏馬力)

=75 kgf·m/s

=735.499 W

放射能	Bq	Ci
	1	2.70270×10^{-11}
	3.7×10^{10}	1

吸収線量	Gy	rad
	1	100
	0.01	1

照射線量	C/kg	R
	1	3876
	2.58×10^{-4}	1

線量当量	Sv	rem
	1	100
	0.01	1

(86年12月26日現在)

Nuclear Data Evaluation for ^{237}Np, ^{241}Am, ^{242g}Am and ^{242m}Am Irradiated by Neutrons and Protons at Energies up to 250 MeV